

Laser Frequency Stabilization for Narrow Linewidth Cooling of ${}^6\text{Li}$

A Senior Honors Thesis

Presented in Partial Fulfillment of the Requirements for graduation
with research distinction in Physics in the undergraduate colleges
of The Ohio State University

by

Adam Reed

The Ohio State University
March 2011

Project Advisers:

Professor Randy Hulet, Rice University, Department of Physics and Astronomy
Professor Nandini Trivedi, Ohio State University, Department of Physics

Copyright © 2011 Adam Reed

PUBLISHED BY ADAM REED

E-MAIL: reed.776@osu.edu

TUFTE-LATEX.GOOGLECODE.COM

Licensed under the Apache License, Version 2.0 (the "License"); you may not use this file except in compliance with the License. You may obtain a copy of the License at <http://www.apache.org/licenses/LICENSE-2.0>. Unless required by applicable law or agreed to in writing, software distributed under the License is distributed on an "AS IS" BASIS, WITHOUT WARRANTIES OR CONDITIONS OF ANY KIND, either express or implied. See the License for the specific language governing permissions and limitations under the License.

First printing, March 2011

Contents

<i>Abstract</i>	7
<i>Introduction</i>	9
<i>Background</i>	13
<i>Laser frequency stabilization</i>	31
<i>Experiment</i>	37
<i>Results</i>	51
<i>Appendix</i>	55
<i>Bibliography</i>	61

List of Figures

1	Quantum Gas	10
2	Rabi oscillations	16
3	Sinc function	16
4	Optical Bloch equations	19
5	Power broadening	20
6	Vapor cell	20
7	Atom-light interactions	22
8	Scattering force on atoms	23
9	Optical molasses cartoon	23
10	Optical molasses force	24
11	Lithium energy levels	27
12	Fine and hyperfine splittings in ${}^6\text{Li}$	27
13	${}^6\text{Li}$ transitions	29
14	Trap and repump	29
15	Doppler-shifted radiation	32
16	Doppler-free setup	33
17	Hole burning	33
18	Population densities with pump and probe beams.	34
19	Cartoon of absorption signal	34
20	Absorption signals	34
21	Gaussian and Lorentzian lineshapes	35
22	Error signals	35
23	Lineshapes	36
24	Overhead view of the home-built modulation circuitry	39
25	Lock-in bandpass filter	41
26	Overhead view of the home-built lock-in amplifier circuitry	42
27	Equivalent circuit of a photodiode	42
28	Picture of the photodiode amplifier	42
29	Response of transimpedance amplifier	43
30	Cartoon of the AOM	43
31	Calibration of the VCO	44

32	Risetimes of the lock-in amplifiers	44
33	Schematic of the optical setup	45
34	Heatpipe pressure	45
35	Scope capture of the RC effects in the absorption signal	45
36	Doppler-free spectrum of ${}^6\text{Li}$ (commercial lock-in)	46
37	Doppler-free spectrum of ${}^6\text{Li}$ (home-built lock-in)	46
38	Long exposure (about 45 sec) of the optical setup	47
39	Doppler-free spectrum without DC offset	48
40	Error signal from Fabry-Pérot cavity	48
41	Schematic of the laser stabilization system	49
42	Lithium-6 vapor cell	49
43	Laser stabilization signal	51
44	Lock signal with triangle wave	51
45	Locked laser linewidth	52
46	Tuning Range of Lock	52
47	${}^{\text{o}}\text{th}$ order signal	52
48	Power spectrum of noise	54
49	Modulation circuit	56
50	Filter circuit	57
51	Transimpedance amplifier	57
52	Summing circuit inside the modulator box	58
53	VCO and RF amp	59
54	Demodulation circuit	60

List of Tables

1	Transition rates	29
2	${}^6\text{Li}$ cooling limits	29
3	Measurements of AOM efficiency	44

Abstract

Laser cooling to micro-Kelvin temperatures requires a laser with active frequency stabilization. The linewidth Γ of an atomic transition sets a lower bound on the Doppler cooling temperature $k_B T_D = \hbar\Gamma/2$. The $2s - 2p$ transition in ${}^6\text{Li}$ has a lower bound temperature of $T_D \approx 140 \mu\text{K}$. In contrast, the $2s - 3p$ transition has a narrower linewidth and thus provides a lower temperature limit of $T_D \approx 20 \mu\text{K}$. We present a method for stabilizing a laser to an atomic line in a vapor cell using modulation transfer spectroscopy and a home-built lock-in amplifier. Our results demonstrate successful locking of a 323 nm laser to the $2s - 3p$ transition. The stabilized laser provides a second stage of magneto-optical trapping that results in a factor of ~ 5 increase in the phase space density before evaporating to degeneracy in an optical dipole trap¹.

¹ Adam Reed. Laser frequency stabilization for narrow linewidth cooling of ${}^6\text{Li}$ atoms. American Physical Society Conference, Session W45, March 2011

Introduction

Ultracold atomic physics

Atoms and molecules exhibit strange and fascinating phenomena at temperatures near absolute zero. At such cold temperatures, atoms can no longer be thought of as classical billiard balls. Instead, quantum mechanical effects become dominate and new phenomena emerge. For example, numerous groups have used elements such as rubidium and lithium-7 to create a Bose Einstein Condensate (BEC), a unique state of matter that does not occur at room temperature. This phase transition is analogous to water freezing into ice, but it is entirely due to quantum mechanical effects. A degenerate Fermi gas that uses lithium-6 is a similar example of a new phase of matter at ultracold temperatures. These exotic systems have remarkable properties that are useful for understanding diverse phenomena ranging from superfluidity and superconductivity to the extreme density of neutron stars. Furthermore, scientists are working on developing optical lattice emulators that simulate complex condensed matter systems in a well-controlled environment².

However, cooling atoms to ultracold temperatures requires techniques that uses lasers to slow atoms down in their tracks. The average kinetic energy, related to translational motion, sets the temperature of the atoms. Laser cooling uses the radiation pressure of light to trap and slow down atoms, bringing their temperature typically down to the milli and micro-Kelvin regime. To achieve sufficient cooling, the wavelength of the lasers must be precisely tuned so that the atom absorbs the laser light. Although further techniques can cool an atomic sample down to a few nano-Kelvin and even lower, laser cooling usually serves as a first stage in reaching the nano-Kelvin regime.

It is advantageous to cool to the lowest possible temperature with laser cooling because the number density of atoms in the quantum degenerate state will increase. For a dilute ideal gas of massive particles in equilibrium, the thermal de Broglie wavelength serves as a measure

² M. Greiner et al. *Nature*, 415:39–44, 2002

of the delocalization of atoms, given by

$$\lambda_{dB} = \frac{h}{\sqrt{2\pi m k_B T}} \quad (1)$$

where h is Planck's constant, m is the mass of a gas particle, k_B is Boltzmann's constant, and T is the equilibrium temperature of the gas. Roughly speaking, the de Broglie wavelength describes the size of a region in which an atom would be found upon measuring its position. A cartoon of a classical and quantum gas is shown in Figure (1).

We can use the de Broglie wavelength to determine the conditions at which quantum effects become dominate. Let the number density of gas particles be $n = N/V$ where N is the total number of particles and V is the total volume they occupy. We then define the phase space density to be $\rho \equiv n\lambda_{dB}^3$. When the de Broglie wavelength is roughly equal to or less than the interparticle spacing

$$\left(\frac{V}{N}\right)^{1/3} \leq \lambda_{dB} \quad (2)$$

the quantum nature of the gas will become dominant, where the interparticle spacing is approximated to be $(V/N)^{1/3}$. In terms of the phase space density, the gas will obey Bose-Einstein statistics or Fermi-Dirac statistics when $\rho \geq 1$. In contrast, the gas can be described by a Maxwell-Boltzmann distribution when $\rho \leq 1$. In other words, the gas is classical and quantum effects are not evident.

Summer research at Rice University

In this thesis, I report on a system that I built used to precisely stabilize the wavelength of the laser to an atomic transition in lithium-6. The linewidth Γ of an atomic transition sets a lower bound on the Doppler cooling temperature $k_B T_D = \hbar\Gamma/2$. The $2s - 2p$ (red) transition in ${}^6\text{Li}$ has a lower bound temperature of $T_D \approx 140 \mu\text{K}$. In contrast, the $2s - 3p$ (ultra-violet) transition has a narrower linewidth and thus provides a lower temperature limit of $T_D \approx 20 \mu\text{K}$. The stabilized laser provides a second stage of laser cooling that will increase phase space density of ${}^6\text{Li}$ atoms before evaporating to degeneracy in an optical dipole trap. The temperature limit is reduced by a factor of seven, so the phase space density $\rho \sim 1/T^{3/2}$ will be increased by a factor of ~ 20 . Based on experimental results (from the Hulet group) of cooling ${}^6\text{Li}$ using the red transition, the minimum temperature limit is roughly double the Doppler-limit. Thus, we expect a minimum cooling temperature of $\sim 40 \mu\text{K}$ and roughly an order of magnitude increase of the phase space density.

I used modulation transfer spectroscopy together with a home-built lock-in amplifier to stabilize the laser frequency (i.e. wavelength)³ The

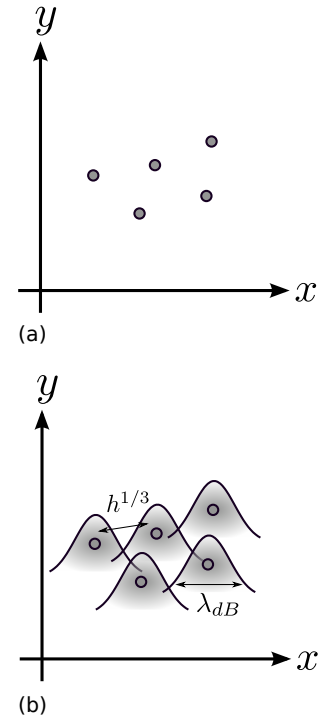


Figure 1: (a) Ideal gas with non-interacting particles at room temperatures. The space between the particles is much greater than their typical wavefunctions. (b) Quantum gas of non-interacting particles. The de Broglie wavelength λ_{dB} is comparable to the inter-particle spacing. For example, air molecules have an average distance of 3 nm and at room temperature $\lambda_{dB} \sim 0.02 \text{ nm}$, so quantum effects are not present. However, for an electron at room temperature, $\lambda_{dB}^3 = (4.3 \text{ nm})^3$. The volume of an atom in metal with one conduction electron per ion is roughly $(0.2 \text{ nm})^3$. Thus, the electrons in a metal form a quantum degenerate gas in which Boltzmann statistics do not apply.

³ To get a feeling for the numbers, in this experiment, the variance of the laser frequency must be roughly less than $\Gamma/2 \sim 400 \text{ kHz}$. Thus, for 323 nm light, the laser frequency must be stable to within 400 kHz of 1000 THz (323 nm), or roughly one part in 10^9 !

technique of modulation transfer spectroscopy generates precise signal to stabilization the laser frequency. I modulated part of the laser beam by using a acoustic-optical modulator (AOM) and a home-built modulation circuit. To recover the lock signal from the noise environment, I designed and built a lock-in amplifier from off-the-shelf analog components. I then implemented these elements into a saturation absorption spectroscopy setup. Finally, I optimized the optical elements in the experiment to improve the signal to noise ratio.

Our results demonstrate successful locking of a 323 nm laser to the $2s - 3p$ transition in lithium-6. I measured the power spectrum of the stabilization system and found no significant sources of noise from the electronics. I also determined the stability of the lock by changing the laser frequency and observing the response of the feedback electronics. As a crude test, I found the lock was impervious to small perturbations such as tools falling on the optical table, doors gently closing (i.e. slamming), and other things that are common in an experimental physics lab. Such stability is crucial to a laser cooling experiment that might last a few hours or longer.

Roughly a month after my project was completed, my laser stabilization system was successfully used in an atom cooling experiment. The UV laser was stabilized to the narrow $2s - 3p$ transition in lithium-6. Part of the beam from the stabilized laser was used to create a magneto optical trap (MOT) to cool the lithium-6 atoms. This UV MOT successfully cooled atoms to roughly $61 \mu\text{K}$ with a factor of ~ 5 improvement of the phase space density.

Organization of thesis

This thesis summarizes my summer project at Rice University and also contains some background relevant to my project. The chapters are organized as follows:

1. **Background** starts off studying a simple two level quantum system. The purpose of this section is not to present rigorous derivations, but rather motivation towards understanding how atoms interact with an optical field and how laser light can be used to cool atoms. The background section concludes with basic electronic properties of lithium-6 and inherent characteristic temperatures experience in laser cooling of lithium-6.
2. **Laser frequency stabilization** describes how a clever technique in non-linear optics⁴ can be used to stabilize the absolute laser frequency of a laser used in atom cooling.
3. **Experiment** goes into the details of the design and implementation of the laser stabilization setup. The section includes details of the home-built electronics.
4. **Results** presents our data that demonstrate successful locking to the $2s - 3p$ transition in lithium-6. Possible improvements on the stabilization system are proposed.
5. **Appendix** contains schematics for the electronics and also a list of parts/equipment.

⁴ Saturated Absorption Spectroscopy

Acknowledgements

I would like to thank Pedro Duarte for spending a lot of his time helping Kevin and I with our projects⁵. I would also like to thank Dr. Bruce Johnson for hosting the REU program at Rice University and Dr. Randy Hulet for supervising me this summer. I would also like to thank my co-adviser Dr. Nandini Trivedi. Finally, I would like to thank Drs. Jennifer Johnson and Louis DiMauro for being on my thesis committee.

⁵ Pedro also read the first few (!) drafts of my thesis—I’m grateful for his comments.

This work was co-supported by the NSF REU program (Physics and Chemistry and DMR) and the DoD ASSURE program. I would also like to thank the Pressey Honors Endowment and Dr. Hulet for funding my trip to the March 2011 American Physical Society conference in Dallas, Texas.

Background

Laser cooling and trapping refers to reducing the velocity of atoms to near zero (“cooling”) and confining the atoms to a particular point in space (“trapping”). The primary force used to trap and cool comes is a result of the momentum transfer from photons scattering off an atom. This momentum transfer is similar to bombarding a bowling ball by a stream of ping pong balls—in both cases the momentum transfer from each scattered particle is tiny⁶. However, if a strong atomic transition is excited, it may be possible to scatter more than 10^7 photons per second, thereby resulting in relatively large accelerations ($10^4 g$) which can be used to manipulate atoms using laser beams.

This chapter goes into the detail of laser cooling and trapping by motivating introductory concepts of light-matter interactions. We consider a simple a two-level atom immersed in a classical oscillating electric field. This model is *semiclassical* because the atom is treated quantum mechanically and the radiation is treated as a classical field. Solving this two-level system gives us valuable insight information about decay rates, transition rules, dampening, and population levels of the two states. To understand the nature of absorption and spontaneous emission of radiation, we use Einstein’s A and B coefficients. We then study the time evolution of the populations and coherences for the two levels are described by the *optical Bloch equations*. After motivating light-matter interactions with a two-level system, we go over laser cooling and its characteristic temperatures. This section represents a summary of the physics that I learned while working on my project. Much of the material here summarizes sections in Metcalf⁷ and Foot⁸; the reader is encouraged to check out these excellent sources for further reading.

For a personal account of the development of laser cooling and trapping, the Nobel lectures by Steven Chu⁹, Claude Cohen-Tannoudji¹⁰, and William Phillips¹¹ are a great resource.

⁶ A ${}^6\text{Li}$ atom at room temperature moves at $\sim 10^5$ cm/sec, roughly the speed of a bullet. To cool down to a few micro-Kelvin, the atom’s velocity needs to be reduced to roughly 10 cm/sec.

⁷ Harold Metcalf. *Laser Cooling and Trapping*. Springer, 1999

⁸ C. J. Foot. *Atomic Physics*. Oxford University Press, 2005

⁹ Steven Chu. The manipulation of neutral particles, December 1997

¹⁰ Claude N. Cohen-Tannoudji. Manipulating atoms with photons, December 1997

¹¹ William D. Phillips. Laser cooling and trapping of neutral atoms, December 1997

Two-level system

Start with a two-level quantum system with energy levels E_1 and E_2 . Our goal is to see how this system evolves with an applied oscillating electric field. The Hamiltonian is given by

$$H = H_0 + H'(t) \quad (3)$$

where H_0 describes the field-free atom and $H'(t)$ is a perturbation due to a classical oscillating electric field. The atomic Hamiltonian has eigenvalues $E_n = \hbar\omega_n$ and eigenfunctions $\psi_n(\mathbf{r})$ for energy levels $n = 1$ and 2 . The time-evolution of the wavefunction is calculated by the time-dependent Schrödinger equation

$$i\hbar \frac{\partial}{\partial t} \Psi(\mathbf{r}, t) = H\Psi(\mathbf{r}, t) \quad (4)$$

where $\Psi(\mathbf{r}, t)$ is the wavefunction and \mathbf{r} is the position of the electron with respect to the atom's center of mass. The wavefunctions at any time t are made up of a linear combination of the stationary states

$$\Psi(\mathbf{r}, t) = c_1(t)\psi(\mathbf{r})e^{-iE_1 t/\hbar} + c_2(t)\psi(\mathbf{r})e^{-iE_2 t/\hbar} \quad (5)$$

where $c_n(t)$ are constants determined by the boundary conditions. Normalization requires that $|c_1|^2 + |c_2|^2 = 1$. We can re-write Ψ in the more compact form

$$\Psi(\mathbf{r}, t) = c_1|1\rangle e^{-i\omega_1 t} + c_2|2\rangle e^{-i\omega_2 t} \quad (6)$$

by representing the eigenfunctions $\psi_n(\mathbf{r})$ with ket notation $|n\rangle$, setting $c_n(t) \equiv c_n$, and writing the energy in terms of angular frequency $\omega_n = E_n/\hbar$.

We now immerse the atom in a classical oscillating electric field $\mathbf{E} = \mathbf{E}_0 \cos(\omega t)$. This radiation produces a perturbation given by

$$H'(t) = -e\mathbf{r} \cdot \mathbf{E}_0 \cos(\omega t) \quad (7)$$

which corresponds to the energy of an electric dipole $-e\mathbf{r}$ in an electric field. By absorbing the diagonal elements of $H'(t)$ into H_0 and putting 5 into 4, we

$$\begin{aligned} i\hbar c'_1(t) &= c_2(t)H'_{12}(t)e^{-i\omega_0 t} \\ i\hbar c'_2(t) &= c_1(t)H'_{21}(t)e^{i\omega_0 t} \end{aligned} \quad (8)$$

where $H'_{ij}(t) \equiv \langle i|H'(t)|j\rangle$ for i, j labeling each state and $\omega_0 \equiv \omega_2 - \omega_1$. Equations (8) are equivalent to the time-dependent Schrödinger equation. Our task is to use suitable approximations to solve these equations for $c_1(t)$ and $c_2(t)$ to give us the probability as a function of time for the atom to be in the excited state.

The first approximation we make is the **dipole approximation**. We assume the radiation has a wavelength λ much greater than the size of the atom a_0 (the Bohr radius), so $\lambda \gg a_0$. This approximation allows us to assume the electric field is nearly uniform over the entire atom¹². Thus, the coupling matrix elements between the two states are given by

$$H'_{ij}(t) = \hbar\Omega \cos(\omega t) \quad (9)$$

where the **Rabi frequency** is defined to be

$$\Omega = \frac{-eE_0}{\hbar} \langle 2|r|1\rangle. \quad (10)$$

that we took E_0 outside of the integral

$$\langle 2|\mathbf{r} \cdot \mathbf{E}_0|1\rangle = \int \psi_2^*(r)\mathbf{r} \cdot \mathbf{E}_0\psi_1(r)d^3\mathbf{r} = E_0\langle 2|r|1\rangle \quad (11)$$

since $|\mathbf{E}_0| = E_0$ is assumed to have no spatial dependence.

The second approximation we make is the **rotating wave approximation**. We assume the radiation has a frequency ω that is close to the atomic resonance ω_0 , so that $|\omega - \omega_0| \ll 1$ and $\omega + \omega_0 \approx 2\omega_0$. Thus we can neglect terms of order $1/\omega$ compared to terms of order $1/\delta$ where the laser detuning is define by $\delta = \omega - \omega_0$.

We uncouple equations (8) by differentiating each on and making two differential equations for c_1 and c_2

$$\begin{aligned} c_1''(t) - i\delta c_1'(t) + \frac{\Omega^2}{4}c_1(t) &= 0 \\ c_2''(t) + i\delta c_2'(t) + \frac{\Omega^2}{4}c_2(t) &= 0 \end{aligned} \quad (12)$$

Assume the atom starts off in the ground state, so the initial conditions are $c_1(0) = 1$ and $c_2(0) = 0$. The solutions to (12) are given by

$$c_1(t) = \left(\cos \frac{\Omega'}{2} - i \frac{\delta}{\Omega'} \sin \frac{\Omega' t''}{2} \right) e^{i\delta t/2} \quad (13)$$

and

$$c_2(t) = -i \frac{\Omega}{\Omega'} \sin \left(\frac{\Omega' t}{2} \right) e^{-i\delta t/2} \quad (14)$$

where $\Omega' \equiv \sqrt{\Omega^2 + \delta^2}$. Figure shows the plot of $|c_2(t)|^2$ for different values of Ω and δ . We find that the populations between the two levels oscillate at Ω' . that as the detuning $|\delta|$ increases, the frequency of oscillation increases but the amplitude decreases. For $t = \pi/\Omega'$, the entire population is in the upper state. A plot of the Rabi oscillations for a two level system is shown in Figure ()�.

¹² For example, optical wavelengths are typically $\sim 300 - 800$ nm where the Bohr radius for the hydrogen atom is $a_0 \sim 10^{-3}$ nm. In addition, for larger atoms, the wavefunctions are typically contained within a sphere of radius ~ 1 nm.

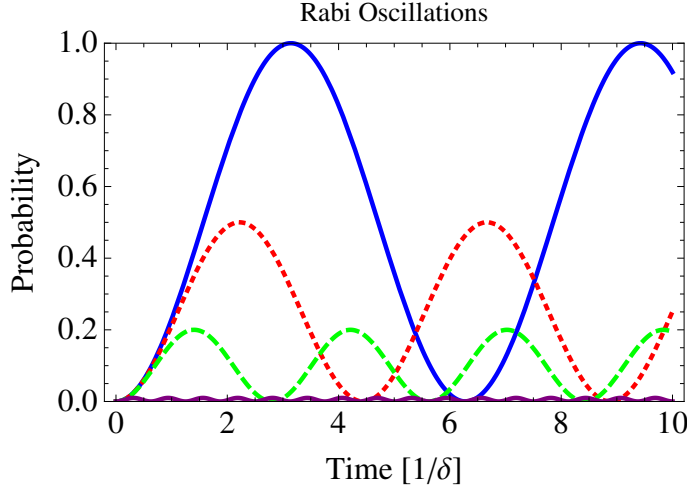


Figure 2: Plot of the probability $|c_2(t)|$ of the atom to be in the excited state for $\Omega = 1$ and $\delta = 0$ (solid blue), 1 (dotted red), 2 (dashed green), and 10 (solid purple). Time units are in $1/\delta$. For near resonant light, the probability to be the upper level oscillates between 0 and 1. As the detuning increases, the frequency of the oscillations increases, but their overall intensity diminishes.

Einstein A and B coefficients

To calculate the probability the atom will be in the excited state, we assume a monochromatic source. However, we now assume a broadband radiation source and use Einstein's treatment of the two-level system to calculate the rate of spontaneous emission of photons from the atom. From Einstein's coefficients, we then calculate the lifetime of the excited state.

Suppose we have a broadband radiation source of energy density $\rho(\omega)$ in the frequency interval ω to $\omega + d\omega$. The amplitude of the applied electric field $E_0(\omega)$ is given by $1/2\epsilon_0 E_0(\omega)^2 = \rho(\omega)d\omega$. Using equation (10), the Rabi frequency then becomes

$$|\Omega|^2 \propto |E_0(\omega)|^2 = \frac{2}{\epsilon_0} \rho(\omega) d\omega. \quad (15)$$

$c_2(t)$ over a range of frequencies to obtain the excitation probability for broadband radiation. Using the rotating wave approximation, for $c_2 \ll 1$ we have

$$|c_2(t)|^2 = \frac{1}{4} |\Omega|^2 t^2 \frac{\sin^2 x}{x^2} \quad (16)$$

using the change of variables $x \equiv (\omega - \omega_0)t/2$.

This expression gives us $|c_2|^2 \propto |\Omega|^2$. We now integrate over a broad range of frequencies

$$|c_2(t)|^2 \propto \int \rho(\omega) \frac{\sin^2(\omega - \omega_0)t/2}{(\omega - \omega_0)^2} d\omega. \quad (17)$$

As time increases, this function becomes sharply peaked at ω_0 as seen in Figure (3). Our range of integration must be sufficiently large compared to the sinc function. In the neighborhood of ω_0 where the sinc function peaks, the smooth function $\rho(\omega)$ can be approximated to be

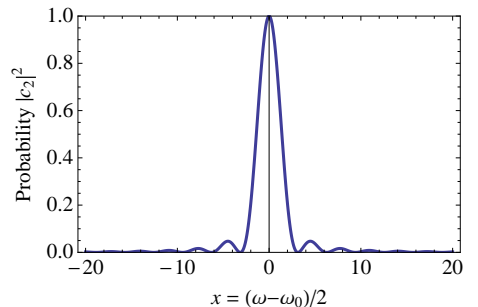


Figure 3: Plot of the probability versus x . Since the sinc function is sharply peaked at the resonant frequency ω_0 , we can approximate it to be a delta function.

a constant $\rho(\omega_0)$ which can be taken out of the integral. Thus we have

$$|c_2(t)|^2 \propto \rho(\omega_0) \times t \int \frac{\sin^2}{x^2} dx. \quad (18)$$

Because the square of the sinc function does not have any appreciable value away from ω_0 , we extend the limits of integration to infinity, which leaves us with the integral $\int_{-\infty}^{\infty} x^{-2} \sin^2(x) dx = \pi$. Dividing through by time t , and including the appropriate factors, we arrive at the transition rate between the two levels

$$R_{12} \equiv \frac{|c_2(t)|^2}{t} = \frac{\pi e^2 |\langle 2|r|1\rangle|^2}{\epsilon_0 \hbar^2} \rho(\omega_0). \quad (19)$$

Comparing this result with Einstein's treatment of radiation, we obtain formulas for the A and B coefficients

$$B_{12} = \frac{\pi e^2 |\langle 2|r|1\rangle|^2}{3\epsilon_0 \hbar^2} \quad (20)$$

and

$$A_{21} = \frac{4\alpha}{3c^2} \times \omega^3 \times |\langle 2|r|1\rangle|^2 \quad (21)$$

where $\alpha = e^2/\hbar c$ $4\pi\epsilon_0 \approx 1/137.1$ is the fine-structure constant.

Optical Bloch Equations

Up to this point, we solved the two-level system for the coherent evolution of the amplitudes for an atom coupled to a oscillating electric field. However, this model does not take into account the important effect of spontaneous emission, which occurs when an atom in the excited state decays to a lower level without being stimulated¹³. Let's go back to the two level system and assume only spontaneous emission. The population of the excited state is N and the rate at which N decays is given by

$$N(t) = N(0)e^{-A_{21}t} \equiv N(0)e^{-\Gamma t} \quad (22)$$

where $N(0)$ is the number of atoms initially in the excited state and Γ is the radiative decay rate. We then have the mean life time of the state τ given by

$$A_{21} = \Gamma = \frac{1}{\tau}. \quad (23)$$

Our task now is to re-write the equations that describe the time evolution of the transition amplitude to include the effect of spontaneous emission. These new set of relations are called the **optical Bloch equations** and they describe the two-level system taking into account spontaneous emission.

In our two-level atom, all the information about the state of the system is represented by the wavefunction $|\Psi\rangle$, a single mathematical object known as a *ket*¹⁴. Experimentally, one cannot measure $|\Psi\rangle$

¹³ In other words, the atom did not absorb a photon prior to decaying back into the lower state. In free space, vacuum fluctuations are the culprit for spontaneous emission.

¹⁴ This object is an element of a **Hilbert space**, a complex vector space with a complex inner product defined such that $\langle \Psi_1 | \Psi_2 \rangle = \langle \Psi_2 | \Psi_1 \rangle^*$ where $*$ is the complex conjugate operation.

directly because it is not an observable quantity. Instead, one measures the expectation value (average value) of a quantum mechanical operator \hat{A} given by

$$\langle \hat{A} \rangle = \langle \Psi | \hat{A} | \Psi \rangle \quad (24)$$

where \hat{A} is a physical observable¹⁵, such as momentum or position. A fundamental difference between quantum mechanics and classical mechanics is the result of our measurement. After performing a certain measurement, one arrives at a probability distribution which is determined completely by the quantum state and the observable describing the measurement. Thus, we have the requirement that our wavefunction be normalized $|\langle \Psi | \Psi \rangle|^2 = 1$.

An important aspect of quantum mechanics is that states can either be pure or mixed. The wavefunction $|\Psi\rangle$ is a pure state and cannot be represented as a mixture of other states. In other words, a **pure state** has all the information about a system stored in one single ket vector. In contrast, a **mixed state** is a statistical mixture of several states. All the information about a mixed state cannot be represented by a single ket vector.

To represent a mixed state, we introduce another mathematical object called the **density matrix** given by

$$\rho = \sum_{s=1}^n p_s |\psi_s\rangle \langle \psi_s| \quad (25)$$

where n is the number of wavefunctions that completely span the Hilbert space and p_s is the fraction of the total ensemble in each pure state $|\psi_s\rangle$. For a pure state, the density matrix is given by

$$\rho = |\psi\rangle \langle \psi| \quad (26)$$

which is the outer product of the ket vector¹⁶. For the two-level system, the density matrix is

$$\rho = (c_1^* c_2^*) \begin{pmatrix} c_1 \\ c_2 \end{pmatrix} = \begin{pmatrix} |c_1|^2 & c_1 c_2^* \\ c_2 c_1^* & |c_2|^2 \end{pmatrix} = \begin{pmatrix} \rho_{11} & \rho_{12} \\ \rho_{21} & \rho_{22} \end{pmatrix} \quad (27)$$

where the off-diagonal elements are called the **coherences**, which represent the response of the system at some driving frequency. The diagonal elements $|c_2|^2$ and $|c_1|^2$ are the **populations**, which as we saw before are the probabilities to be in either of the two states. To summarize, we rewrote the state of a quantum system in terms of the density matrix so that we could handle both pure and mixed states. Our next step is to calculate the time evolution of the density matrix so that we can see how the coherences and the populations of the system evolve over time given a set of initial conditions.

¹⁵ \hat{A} is an operator, denoted by the hat. Throughout the rest of the text, we drop the hat so that $\hat{A} \rightarrow A$.

¹⁶ For a given ket vector $|\Psi\rangle$, there is a corresponding bra vector $\langle \Psi | \equiv |\Psi\rangle^\dagger$, which is the Hermitian conjugate of the original ket vector.

An equivalent form of the Schrödinger equation is given by the von Neumann equation

$$i\hbar \frac{d\rho}{dt} = [H, \rho] \quad (28)$$

where the brackets denote the commutator $[A, B] = AB - BA$ of two operators. First, to simplify the differential equations, we want to make the following transformation

$$u = \rho_{12}e^{-i\delta t} + \rho_{21}e^{i\delta t} \quad (29)$$

$$v = -i(\rho_{12}e^{-i\delta t} - \rho_{21}e^{i\delta t}) \quad (30)$$

$$w = \rho_{11} - \rho_{22} \quad (31)$$

where w is the population difference. Note that as before, the total probability must satisfy $\rho_{11} + \rho_{22} = 1$. We now want to take spontaneous emission into account, so we include a dampening factor $\Omega/2$ in the equation describing the population of the upper level

$$\dot{\rho}_{22} = -\Gamma\rho_{22} + \frac{\Omega}{2}. \quad (32)$$

Next, we put the density matrix into equation (28) and apply the transformations given by (31) and then have (note, the in between steps are not shown here!) the optical Bloch equations

$$\begin{aligned} \dot{u} &= \delta v - \frac{\Gamma}{2}u \\ \dot{v} &= -\delta u + \Omega w - \frac{\Gamma}{2}v \\ \dot{w} &= -\Omega v - \Gamma(w - 1). \end{aligned} \quad (33)$$

To recapitulate what just happened, we came up with a set of equations that describe the time evolution of a two-level system in an oscillating electric field close to resonance. In addition, we also include the effect of spontaneous emission. The optical Bloch equations can be solved to give us coherences and populations of the two levels. An example of solutions to the optical Bloch equations is shown in Figure (4).

Saturation, Power Broadening, and Absorption Rate

At times much larger than the lifetime of the upper level (i.e. $t \gg \Gamma^{-1}$), the system reaches a steady-state, given by

$$\begin{pmatrix} u \\ v \\ w \end{pmatrix} = \frac{1}{\delta^2 + \Omega^2/2 + \Gamma^2/4} \begin{pmatrix} \Omega\delta \\ \Omega\Gamma/2 \\ \delta^2 + \Gamma^2/4 \end{pmatrix} \quad (34)$$

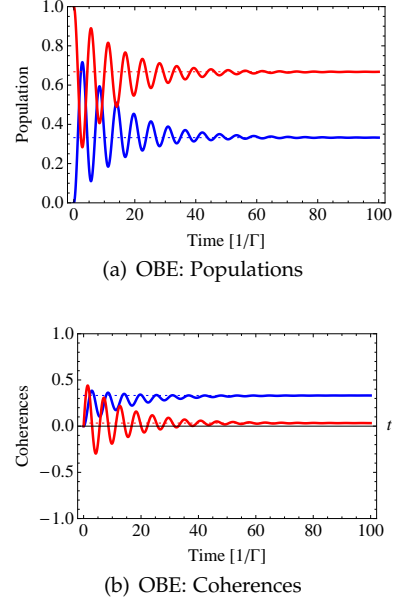


Figure 4: Numerical solutions to the optical Bloch equations (OBE). The optical Bloch equations were solved numerically using *Mathematica* and the `NDSolve[]` command. The initial conditions were such that the atom started out in a pure state, so $u(0) = v(0) = 0$ with the population entirely in the lower level, so $w(0) = \rho_{11} - \rho_{22} = 1$. For $t > 0$, the atom was driven at the Rabi frequency $\Omega = 1$ with an oscillating electric field with a detuning of $\delta = 0.5$. The excited state was assumed to decay at $\Gamma = 0.1$ which causes both the populations and the coherences to reach steady-state values for sufficiently large times. (a) Populations ρ_{22} and ρ_{11} as a function time. Initially, the entire population is in the lower level (red line). For $t > 0$, the populations undergo Rabi oscillations between the two levels. For $t \gg 1/\Gamma$, the populations approach a steady-state (dotted lines). (b) The coherences $\text{Re}[\rho_{12}]$ (red) and $\text{Im}[\rho_{12}]$ (blue) plotted along with their steady-state values. For $t = 0$, the system starts out in a pure state with $\text{Re}[\rho_{12}] = \text{Im}[\rho_{12}] = 0$. The oscillating electric field at $t > 0$ drives the system into a mixed state.

From the above equations, we find the upper level has a steady state population of

$$\begin{aligned}\rho_{22} &= \frac{1-w}{2} = \frac{\Omega^2/4}{\delta^2 + \Omega^2/2 + \Gamma^2/4} \\ &= \frac{s_0/2}{1+s_0+(2\delta/\Gamma)^2}\end{aligned}\quad (35)$$

where the on-resonance **saturation parameter** is defined

$$s_0 \equiv \frac{2|\Omega|^2}{\Gamma^2} = \frac{I}{I_s} \quad (36)$$

and the saturation intensity is given by

$$I_s \equiv \frac{\pi hc}{3\lambda^3\tau} \quad (37)$$

where τ is the lifetime of the state and λ is the wavelength of the incident radiation. We find for $s_0 \gg 1$, the steady state excited population approaches $1/2$. The population in the excited state decays at a rate Γ and in the steady-state, both the excitation rate decay rate are equal, so the total scattering rate is

$$R_{scatt} = \Gamma\rho_{22} = \frac{s_0\Gamma/2}{1+s_0+(2\delta/\Gamma)^2}. \quad (38)$$

At high intensities, the saturation parameter is $s_0 \gg 1$ so $R_{scatt} \rightarrow \Gamma/2$. We can then rewrite the scattering rate as

$$R_{scatt} = \frac{s_0}{1+s_0} \frac{\Gamma/2}{1+(2\delta/\Gamma')^2} \quad (39)$$

where $\Gamma' = \Gamma\sqrt{1+s_0}$ is the power-broadened linewidth of the transition. We find that in addition to the natural linewidth of a transition Γ , we also observe power broadening, which is a result of shortening the lifetime of the upper level due to stimulated emission.

Optical Absorption Cross-section

We now consider the case in which a laser beam passes through an atomic vapor, which is contained in a vapor cell of length L as shown in Figure (6). As the photons from the laser beam pass through the atomic vapor, they will be scattered and the laser beam will be reduced in intensity. If the light is on or near the resonant frequency of the atoms, there will also be spontaneous emission and stimulated emission. Spontaneous emission is isotropic in nature (since the photons are emitted in random directions). In contrast, stimulated emission is directional.

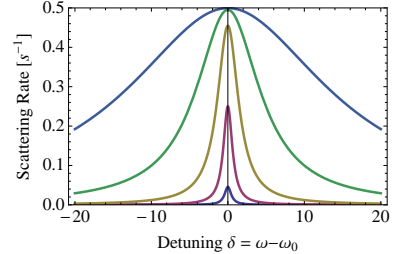


Figure 5: Scattering rate as a function of the laser detuning δ for different values of the saturation parameter s_0 . The excited state decay rate was set to $\Gamma = 1$. The smallest peak corresponds to $s_0 = 0.1$ and the broadest peak corresponds to $s_0 = 1000$. For $s_0 > 1$ the peaks become significantly wider due to power broadening. From plotting the scattering rate for different values of s_0 , we learn that the laser beam should not be too strong (broad lines) or too weak (small peak). Instead, we want the laser power to be just right.

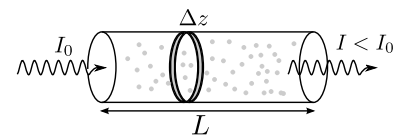


Figure 6: Simple spectroscopy setup. A laser beam with an initial intensity I_0 passes through a cell of length L containing an atomic vapor. For a small segment Δz , the beam intensity diminishes by an amount $-I(\omega)\kappa(\omega)\Delta z$ where κ is the absorption coefficient.

For a small length Δz in the atomic sample along the direction of the laser beam, the corresponding change in intensity is

$$\Delta I(\omega) = -n_1 I(\omega) \sigma(\omega) \Delta z + n_2 I(\omega) \sigma(\omega) \Delta z \quad (40)$$

where σ is the cross-section, which essentially represents the effective area that each atom presents to the laser beam¹⁷. The above equation takes into account both absorption and stimulated emission, which have the same cross-section. We also define the **absorption coefficient** $\kappa(\omega) = (n_1 - n_2)\sigma(\omega)$ which has units of [length⁻¹]. Taking the limit $\Delta z \rightarrow 0$, we get the differential equation

$$\frac{dI(\omega)}{dz} = -\kappa(\omega)I(\omega) \quad (41)$$

which has the solution $I(\omega) = I(0)e^{-\kappa(\omega)L}$ where $I(0)$ is the initial laser beam intensity¹⁸.

Now we will figure out the lineshape of the absorbed laser light. At the steady state condition, conservation of energy requires that the net energy absorbed must equal the energy scattered out of the beam. Thus we have

$$(n_1 - n_2)\sigma I = n_2 A_{21}\hbar\omega \quad (42)$$

which says rate at which absorption exceeds stimulated emission equals the rate at which atoms scatter photon energy. Since the total population density n remains conserved, we have $n = n_1 + n_2$. This expression, together with $\rho_{22} = n_2/n$ and $w = (n_2 - n_1)/n$ allows us to write

$$n_1 - n_2 = \frac{2w}{1-w} \quad (43)$$

so we have

$$\begin{aligned} \sigma &= \frac{2w}{1-w} \frac{A_{21}\hbar\omega}{I} \\ &= \frac{\Omega^2/4}{(\omega - \omega_0)^2 + \Gamma^2/4} \times \frac{A_{21}\hbar\omega}{I} \end{aligned} \quad (44)$$

Since both I and Ω^2 are proportional to $|E_0|^2$, they cancel out and we get (after inserting the appropriate factors)

$$\sigma = \frac{3\pi^2 c^2}{\omega_0^2} A_{21} g_L(\omega) \quad (45)$$

where the **line shape function** is given by the Lorentzian

$$g_L(\omega) = \frac{1}{2\pi} \frac{\Gamma}{(\omega - \omega_0)^2 + \Gamma^2/4} \quad (46)$$

which has units of [sec] and is the same for each atom. Normalization requires

$$\int_{-\infty}^{+\infty} g_L(\omega) d\omega = 1$$

¹⁷ Typically this value is $\sim \lambda^2$.

¹⁸ This solution is valid in the low intensity regime since κ depends on the intensity I .

This lineshape falls under **homogeneous broadening**, which applies to each atom, such as spontaneous emission. In contrast, **inhomogeneous broadening** requires a whole ensemble of atoms, as we will see later for the case of Doppler broadening.

Scattering force

Light can exert forces on matter. Over 400 years ago, Johannes Kepler observed that the tails of comets point away from the Sun, regardless of their orbital position. Kepler explained this phenomenon by proposing that the light from the Sun exerting a force on the dust particles in the comet's tail. In the nineteenth century, James Clerk Maxwell developed his theory of electromagnetism and showed that light is radiation that has both momentum and energy. By conservation of energy, when an object absorbs radiation there is a change in momentum. Newton's law states that the rate of change of momentum equals the force on the object, so the force light exerts on an object equals the rate at which the light delivers momentum. From dimensional analysis, a light beam of intensity I delivers a force on an area A given by¹⁹

$$F_{rad} = \frac{IA}{c} \quad (47)$$

where c is the speed of light. In our everyday lives, the radiation force from light is too feeble to be noticed²⁰. However, the radiation force has a dramatic effect on the motion of microscopic objects.

Lasers can be used to exert controllable forces on atoms. A photon of wavelength λ has a momentum $p = h/\lambda$ where h is Planck's constant. It is convenient to write the momentum as $p = \hbar k$ where $\hbar = h/2\pi$ and $k = 2\pi/\lambda$ is the wavenumber. When an atom absorbs a photon, the atom gains momentum $\hbar k$ in the direction of the incident photon, as shown in Figure (a). The atom will then spontaneously emit a photon in a random direction. After scattering a sufficient number of photons, the atom will experience a net average **scatter force**. This force slows the atom down and equals the rate at which momentum is delivered to the atom by the absorbed photons, or

$$F_{scatt} = \text{photon momentum} \times \text{scattering rate}. \quad (48)$$

A cartoon of a beam of atoms slowed down by light is shown in Figure (b). We found that the scattering rate $R_{scatt} = \Gamma \rho_{22}$. Thus, in the steady state, we have

$$F_{scatt} = \hbar k \frac{\Gamma}{2} \frac{s_0}{1 + s_0 + 4(\delta \pm kv)^2/\Gamma^2} \quad (49)$$

where the $\pm kv$ takes into account the Doppler shift in radiation as observed by an atom traveling at a velocity v along the k direction. Notice

¹⁹ For a reflecting surface, the momentum change is twice as large so the radiation force will be doubled.

²⁰ The light from the sun has an intensity of about 1 kW m^{-2} , so for 1 m^2 on the Earth, the radiation pressure is about $3 \mu\text{N}$. In contrast, for 1 m^2 at 1 atmosphere (atm), the corresponding force is $101,325 \text{ N}$.

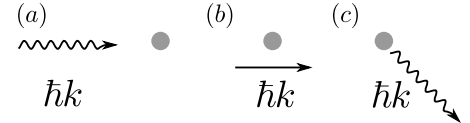


Figure 7: Atom-light interactions. (a) An atom at rest and an incident photon with momentum $\hbar k$. (b) The atom absorbs the photon and is “kicked” in the opposite direction. (c) The atom then emits a photon in a random direction due to spontaneous emission.

that for beams with a strong intensity I , the saturation parameter becomes large and the maximum scattering force is then $F_{max} = \hbar k \Gamma / 2$. The factor of $\Gamma/2$ is a result of the populations in the two level atom reaching $1/2$ at high intensities. For an atom with a mass M , the maximum acceleration is

$$a_{max} = \frac{F_{scatt}}{M} = \frac{\hbar k \Gamma}{2M} = \frac{v_r}{2\tau} \quad (50)$$

where τ is the lifetime of the excited state and the **recoil velocity** is $v_r \equiv \hbar k / M$, which is the atom's new velocity after absorbing or emitting a photon.

The scattering force can be used to slow down a beam of atoms. Suppose we have an oven that heats up an atomic sample, thus producing a beam of atoms moving at a velocity v . A laser produces photons with a wavenumber k moving toward the atoms. The laser beam is **red detuned** because the frequency of the light is tuned down by an amount $-kv$ to account for the Doppler-shifted radiation as observed by the moving atoms. This detuning is necessary because the photons must be near the atom resonance to be absorbed by the atom. Each absorbed photon gives the atoms a kick opposite to their original motion and all the scattered photons go off in random directions. The result is a net force on the atoms which slows them down.

To trap and cool a cloud of atoms, laser beams in three orthogonal directions are required as shown in Figure (9). Such a configuration is required because atoms in gas move over all the place in three dimensions. Although the laser beams are all derived from the same source using mirrors, the atoms in the gas do not experience the same radiation force. This imbalance in the forces arises because in moving frame of the atom, the radiation is Doppler-shifted. Since the laser beams are counterpropagating, atoms observe blue shifted light in one direction and red shifted light in the opposite direction. Using equation (49), the imbalance in the forces (dropping the "scatt" subscript on F) is

$$\begin{aligned} F_{tot} &= F(\delta - kv) - F(\delta + kv) \\ &\approx F(\delta) - kv \frac{\partial F}{\partial \omega} - \left[F(\delta) + \delta kv \frac{\partial F}{\partial \omega} \right] \\ &= -2kv \frac{\partial F}{\partial \omega} \end{aligned} \quad (51)$$

where F was expanded assuming low velocities $kv \ll \Gamma$. We can rewrite the above equation as $F_{tot} = -\alpha v$ where α is a dampening coefficient as if the atoms were in some sort of viscous fluid. Computing α , we find

$$\alpha \approx 4\hbar k^2 s_0 \frac{-2\delta/\Gamma}{[1 + (2\delta/\Gamma)^2]^2} \quad (52)$$

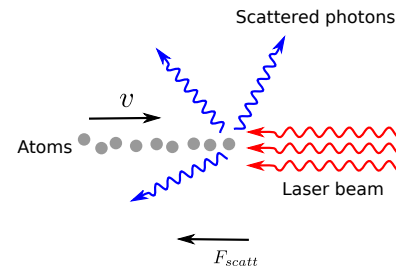


Figure 8: Slowing down atoms using the scattering force. An oven produces a beam of atoms moving at a velocity v . Incident laser light is red detuned (red wiggles) at a frequency such that in the atoms' frame, the light is on resonance. The atoms scatter photons in random directions, but there is a net scattering force in the $-v$ direction.

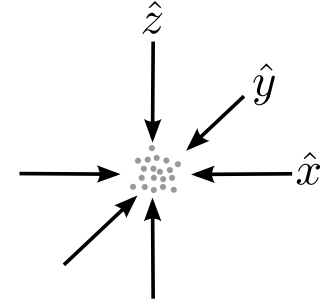
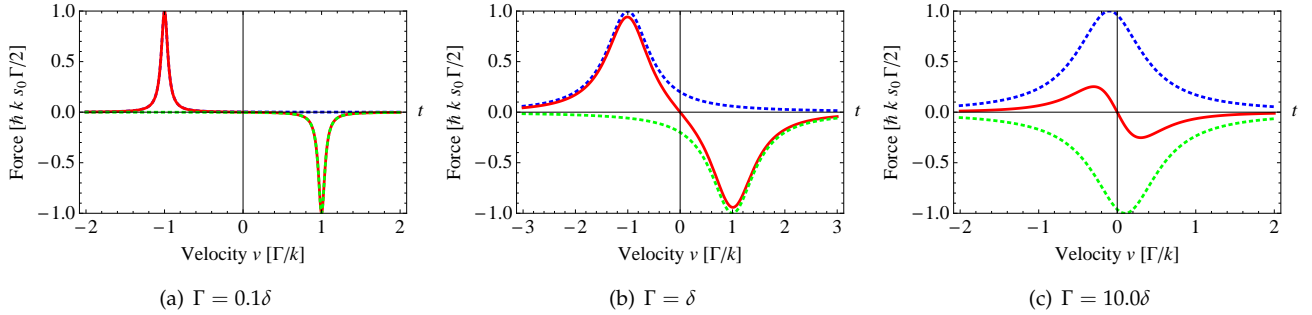


Figure 9: Cartoon of a cloud of atoms in an optical molasses. The arrows represent counterpropagating laser beams in three orthogonal directions. The laser beams are all derived from the same source, made possible by a clever arrangement of mirrors (not shown). This setup is a simple optical trap that makes it possible to confine and cool atoms.

where we assumed a weak beam, so $s_0 \ll 1$ gets ignored. In order for dampening to occur, $\alpha > 0$ which implies $\delta < 0$ so we need red detuned light to achieve cooling. A plot of F_{tot} is shown in Figure () for various parameter values. This laser cooling technique is referred to as **optical molasses** because the damped atoms in the optical field are analogous to a particle in fluid like honey.



Characteristic temperatures in laser cooling

In laser cooling, temperature labels the average kinetic energy of an atomic sample²¹ The equipartition theorem relates the temperature of a system to its average energy by

$$\langle E_k \rangle = \frac{1}{2} k_B T \quad (53)$$

where k_B is Boltzman's constant. This notion of temperature requires that the atoms follow a well-defined velocity distribution. For an ideal gas in three dimensions, the atoms follow a Maxwell-Boltzmann distribution, and the temperature is related to the root-mean-squared (RMS) velocity v_{RMS} by

$$v_{RMS} = \sqrt{\frac{3k_B T}{M}} \quad (54)$$

where M is the atomic mass. In the optical molasses technique, the scattering force reduces v_{RMS} , thereby lowering the temperature of the atomic sample. However, laser has intrinsic temperature limits, defined by two important characteristic temperatures: the **Doppler temperature** and the **recoil temperature**.

Ignoring spontaneous emission, the **recoil temperature** T_R describes the temperature associated with the recoil energy of a single photon. An atom that absorbs a photon of momentum $\hbar k$ obtains a recoil velocity v_r that is related to the temperature of the atom. Thus, the recoil

Figure 10: Total scattering force (solid line) on an atom as a function of velocity. The forces that the atom experiences for the left and right beams are also plotted (dotted lines). The wavevector was set to $k = 1$. Observe that for $v < 0$, the force pushes the atom in the positive direction, whereas for $v > 0$, the force is negative and directs the atom back towards the center. For small velocities around $v = 0$, the dampening is proportional to the slope of the line. In (a), the slope of the dampening around $v = 0$ is small, whereas in (c), the slope is larger, but the detuning is small so the individual left and right forces start to cancel. In the limit of zero detuning, the left and right forces exactly cancel.

²¹ **Disclaimer:** temperature in laser cooling is not so easy to define. In thermodynamics, the definition of temperature requires that the system be in some sort of thermal contact with its environment. However, in laser cooling, the atoms are continuously absorbing and scattering light (so the system is no longer closed since the atoms are changing their environment). Moreover, there is no heat exchange between the system (the atoms) and the environment (the optical field). While the system may have reached the steady state, it may not be in thermal equilibrium, so temperature cannot be so easily defined. However, the idea of "temperature" in laser cooling is used more as a label of the average kinetic energy.

temperature is given by

$$k_B T_R = \frac{\hbar^2 k^2}{2M}. \quad (55)$$

where M is the atomic mass. The recoil temperature is typically of order a few μK . However, the atom will spontaneous decay back into the ground state at a rate Γ , which gives rise to the Doppler temperature.

The **Doppler temperature** describes the balance between laser cooling and diffusive heating caused by the random nature of absorption and spontaneous emission of photons²². The total force from a single laser beam can be written

$$\mathbf{F}_{tot} = \mathbf{F}_{absorb} + \delta\mathbf{F}_{absorb} + \mathbf{F}_{spont} + \delta\mathbf{F}_{spont} \quad (56)$$

where \mathbf{F}_{absorb} is the force on the atom due to the absorption of a photon and \mathbf{F}_{spont} describes spontaneous emission. As one would expect, the random kicks due to spontaneous emission average out and give us $\langle \mathbf{F}_{spont} \rangle = 0$. However, the average force due to absorption gives us the scattering force $\langle \mathbf{F}_{absorb} \rangle = \mathbf{F}_{scatt}$. The respective fluctuations on these two forces are $\delta\mathbf{F}_{absorb}$ and $\delta\mathbf{F}_{spont}$, which diabolically contribute to heating of the atoms.

One can estimate the equilibrium temperature in the optical molasses technique by equating the heating and cooling rates. The random kicks an atom receives from scattering photons results in a random walk in momentum space. Each step size of the random walk is equal to the recoil momentum $p_r = \hbar k$. Although the average of the momentum is zero $\langle p \rangle = 0$, the square goes as $\langle p^2 \rangle = (\sqrt{N}p_r)^2$. During a time interval t , the atom will scatter an average number of $N = 2R_{scatt}t$ photons, where R_{scatt} is the scattering rate²³. The heating rate is given by

$$\frac{dE_{heat}}{dt} = \frac{d}{dt} \left(\frac{\langle p^2 \rangle}{2M} \right) = R_{scatt} \frac{p_r^2}{2M} \quad (57)$$

and the cooling rate is given by

$$\frac{dE_{cool}}{dt} = \frac{d}{dt} \left(\frac{1}{2} M v^2 \right) = -\mathbf{F} \cdot \mathbf{v} \quad (58)$$

where \mathbf{F} is the frictional dampening force on the atom in the optical molasses. By equating the heating and the cooling rate, we get the average steady state energy

$$\langle E_{steady} \rangle \propto M p_r \frac{R_{scatt}}{\alpha} \quad (59)$$

where α is the dampening constant. By the equipartition theorem, we know the average kinetic energy of the atom is related to the temperature by

$$\langle E_{kinetic} \rangle = \frac{1}{2} k_B T \quad (60)$$

²² J. Dalibard. *Journal of the Optical Society of America B*, page 2023, 1989. DOI: 10.1029/2002JD002268

²³ The factor of two comes from assuming there are a pair of laser beams, so the rate will be twice that of a single beam.

where k_B is Boltzman's constant. Thus, equating the average kinetic energy with the steady state energy gives us the equilibrium temperature, which is called the **Doppler temperature**. After inserting the appropriate factors, we find

$$k_B T_D = \frac{\hbar\Gamma}{2} \quad (61)$$

where k_B is Boltzman's constant and Γ is the rate of spontaneous emission of the excited state. A minimum temperature of order $\hbar\Gamma$ is reasonable because the heating is determined by the scattering rate, which is proportional to the rate of spontaneous emission from the excited state. The \hbar then gives us the correct units. Typical values for T_D are around a few hundred μK . Although we have derived a minimum theoretical temperature on the optical molasses technique, sub-Doppler cooling mechanisms have been experimentally demonstrated²⁴.

Electronic properties of lithium-6

Naturally occurring lithium appear in the form of two stable isotopes. The more abundant isotope is ${}^7\text{Li}$ (92.5% abundance), which has four neutrons²⁵. In contrast, ${}^6\text{Li}$ has only three neutrons and is much less abundant (7.6% abundance). For the purposes of atom cooling, the main difference between ${}^6\text{Li}$ and ${}^7\text{Li}$ is that these isotopes differ by a single spin-1/2 particle, so they will inevitably exhibit different quantum behavior at ultracold temperatures. In particular, ${}^7\text{Li}$ is a composite boson, so can be cooled to a Bose-Einstein Condensate (BEC). However, ${}^6\text{Li}$ is a composite fermion, so its fate at ultracold temperatures is a degenerate Fermi gas, as set by the Pauli exclusion principle.

Lithium-6 has closed inner shell ($n = 1$) with one lone valence electron. The electronic configuration is $1s^22s^1$, which is for the ground state²⁶. Notice that the valence electron experiences one net positive charge and the inner electrons screen the nucleus to give an effective charge Z_{eff} . As a result of this configuration, the energy levels of ${}^6\text{Li}$ are similar to those of the hydrogen atom.

This simple model of the energy levels of ${}^6\text{Li}$ is the **central-field approximation**, which takes this idea that the energy levels are hydrogen-like and assumes the valence electron is independent. See diagram (??). Moreover, we assume that the nucleus and the closed inner shell electrons produce a spherically-symmetric electric field, simplifying the calculations.

To describe the electronic state of the atoms, we use the hydroglific **term symbols**, which are ubiquitous in atomic physics. The state of the electron configurations are specified by the angular momentum quantum numbers s , ℓ , and j . For multiple electrons, the total orbital angular momentum is $\mathbf{L} = \sum_i \ell_i$ and the total electronic spin is $\mathbf{S} = \sum_i \mathbf{s}_i$.

²⁴ Cohen-Tannoudji and Jean Dalibard demonstrated sub-Doppler cooling by what they dubbed the *Sisyphus* cooling technique.

²⁵ John Emsley. *Nature's Building Blocks*. Oxford: Oxford University Press., 2001. ISBN 0198503415

²⁶ The notation is nl where n is the principle quantum number and ℓ is the orbital electronic angular momentum quantum number. The superscript number refers to how many electrons at in the orbital.

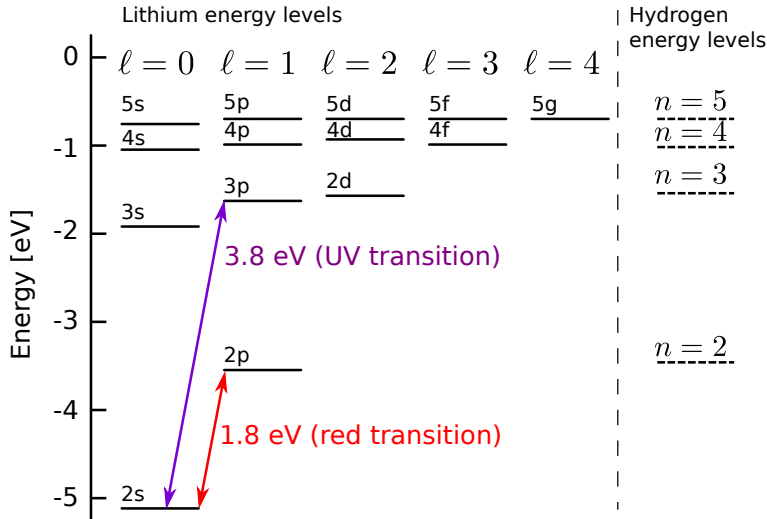


Figure 11: Lithium energy levels. The hydrogen energy levels are shown to the right for comparison. Notice that the angular momentum states have energy levels close to that of hydrogen, but the s and p states fall below. This effect is due to the decreasing penetration of electronic wavefunctions as ℓ increases. For example, the $3d$ electron is most likely to be found well outside of the inner core of electrons, so the energy is similar to that of a hydrogen atom. However, the $3s$ electron penetrates the core inner electrons, thus lowering its energy.

The total electronic angular momentum is $\mathbf{J} = \sum_i \mathbf{j}_i$. Their corresponding magnitudes are given by $L = \hbar\sqrt{\ell(\ell+1)}$, $S = \hbar\sqrt{s(s+1)}$, and $J = \hbar\sqrt{j(j+1)}$. The total angular momentum \mathbf{J} is defined by $\mathbf{J} = \mathbf{L} + \mathbf{S}$. The possible values of the total angular momentum J are given by $|L - S| \leq J \leq (L + S)$.

A term symbol encapsulates this information in the form of

$$^{2S+1}L_J \quad (62)$$

where $2S + 1$ is the multiplicity, the maximum number of J states for a given LS combination. This symbol is also referred to as a Russell-Saunders term, which assumes coupling between the intrinsic angular momentum spin of the valence electron and the orbital angular momentum (LS coupling). The ground and excited states of ${}^6\text{Li}$ are shown in Figure (12) where the spin-orbit coupling is shown to the right. Allowed electric dipole transitions are determined by $\Delta L = 0, \pm 1$. The D_1 and D_2 lines shown are a result of LS coupling.

In the ground state configuration of ${}^6\text{Li}$, the valence electron is in the $2s$ orbital ($n = 2$), so $L = 0$ and $S = 1/2$. The only possible value for the total angular momentum is $J = 0 + 1/2 = 1/2$. Thus, the term symbol is written as ${}^2S_{1/2}$. In the next excited state, the electron is in the $3p$ state, so $L = 1$ and $S = 1/2$ so $J = 3/2, 1/2$, which gives us ${}^2P_{3/2}$. A energy level diagram is shown in Figure (12).

We now write down the total energy for the single valence electron ${}^6\text{Li}$ atom. Assuming an infinitely massive nucleus, the nonrelativistic Hamiltonian is

$$\hat{H} = \underbrace{\frac{p^2}{2\mu}}_K - \underbrace{\frac{Z_{eff}e^2}{4\pi\epsilon_0 r}}_V + \underbrace{\hat{H}_{SO}}_{\text{spin-orbit}} + \underbrace{\hat{H}_{hyp}}_{\text{hyperfine}} \quad (63)$$

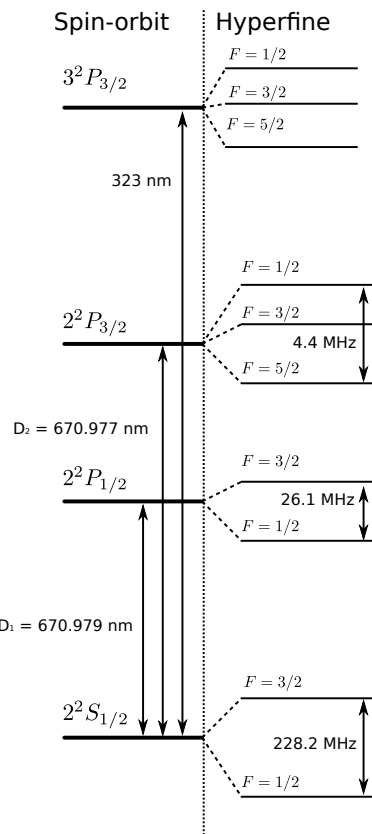


Figure 12: Spin-orbit and hyperfine splittings of lithium-6.

where $\mathbf{p} = -i\hbar\vec{\nabla}$ is the momentum operator and μ is the reduced mass of the electron and nucleus. The total kinetic energy is K and the potential is V determined by Coulomb interaction of the single electron with the nucleus and core electrons (under the central-field approximation). The spin-orbit coupling arises from the magnetic moment of the proton coupling with the spin of the electron. By considering the magnetic coupling of the nucleus and the electron spin, the energies are further split into the hyperfine structure.

Beyond the fine structure of Li is the hyperfine structure. The states are labeled by the quantum number $F = I + J$ which is the total angular momentum of the atom and I is for the spin angular momentum of the nucleus. The allowed values are given by $|J - I| \leq F \leq (J + I)$. Hyperfine splittings are small compared to the fine structure splittings because the nuclear magnetic moment is much weaker than the electron magnetic moment. The nuclei of these isotopes differ by the number of neutrons, so their hyperfine splittings will be different. For ${}^7\text{Li}$, $I = 3/2$ since the nucleus has one more neutrons than ${}^6\text{Li}$, which has $I = 1$. For the both isotopes, there are two hyperfine states in the $2^2S_{1/2}$ state, given by $F = I - 1/2$ and $F = I + 1/2$. The electric dipole transitions are given by $\Delta F = 0, \pm 1$, $\Delta J = 0, \pm 1$, and $\Delta s = 0$.

We can use these results to calculate hyperfine states of the fine-structure levels. For the $2^2S_{1/2}$ level, we have $J = 1/2$ and $I = 1$ so there are two possible values of $F = 3/2, 1/2$. In the $2^2P_{1/2}$ state, there are also two possible values of $F = 3/2, 1/2$. However, in the $2^2P_{3/2}$ state, because of $J = 3/2$, there are three possible values of $F = 5/2, 3/2, 1/2$.

Using second order perturbation theory, one can calculate the hyperfine splittings of ${}^6\text{Li}$ ²⁷. In terms of the quantum numbers I, J and F , the energy of a state (in terms of frequency ν) is given by

$$\nu_F = \nu_J + A \frac{C}{2} + B \frac{3/4C(C+1) - I(I+1)J(J+1)}{2J(2I-1)J(2J-1)} \quad (64a)$$

$$C = F(F+1) - J(J+1) - I(I+1) \quad (64b)$$

where ν_J is the energy of the fine structure state determined by J . The coupling constants A and B account for the dipole and quadrupole interactions of the electrons, respectively.

Laser cooling of lithium-6

Before reaching nano-Kelvin temperatures, the ${}^6\text{Li}$ must be laser cooled to μK temperatures. For the $2S_{1/2} \rightarrow 2P_{3/2}$ transition (requiring 671 nm red light) the linewidth is about 6 MHz. The corresponding Doppler cooling limit is $T_D \sim 140\mu\text{K}$ and the recoil limit is $T_R \sim 3\mu\text{K}$. In

²⁷ P. F. Bernath. *Spectra of Atoms and Molecules*. Oxford University Press, 2005

contrast, for the $2S_{1/2} \rightarrow 3P_{3/2}$ transition (requiring UV light), the linewidth is about 700 kHz. The corresponding Doppler cooling limit is $T_D \sim 17\mu\text{K}$ and the recoil limit is $T_R \sim 15\mu\text{K}$. Although the recoil limiting temperature increases, it does not exceed the Doppler temperature. Cooling ^6Li with the narrow linewidth transition gives an improvement of about a factor of seven over cooling with the red transition. However, the challenge is that the UV laser must be stabilized at the narrow transition. As a rough estimate, the RMS locked linewidth of the laser stabilization system must be less than ~ 700 kHz.

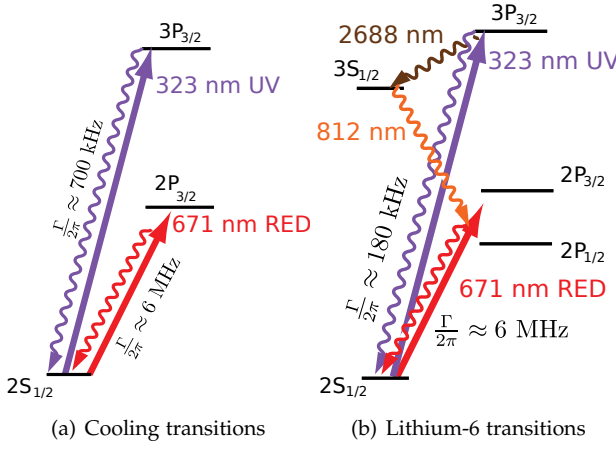


Figure 13: Transitions used for cooling in ^6Li . (a) Red and narrow UV transition and their respective linewidths, taking into account all possible decay paths. (b) The alternate decay paths from the $3s$ to $2s$ states. Diagrams courtesy of Pedro Duarte; modified by the author.

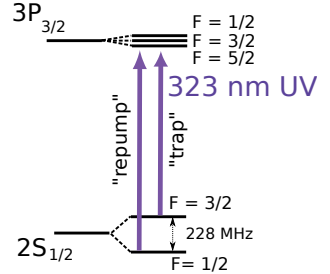


Figure 14: Trap and repump transitions. The hyperfine splitting in the $2S_{1/2}$ between $F = 1/2$ and $F = 3/2$ is about 228 MHz. The hyperfine splitting in the $3P_{3/2}$ is not resolvable in our experiment. **Note:** The terms “trap” and “repump” come from the property of ^6Li that one needs more power for the $F = 3/2$ transition than the $F = 1/2$ to generate a good atom trap.

Transition	Rate $\Gamma [\text{s}^{-1}]$
$3S_{1/2} \rightarrow 2P_{3/2}$	2.33×10^7
$3S_{1/2} \rightarrow 2P_{1/2}$	1.16×10^7
$2P_{3/2} \rightarrow 2P_{1/2}$	3.72×10^7
$2P_{1/2} \rightarrow 2S_{1/2}$	(same as above)
$3P_{3/2} \rightarrow 2S_{1/2}$	1.17×10^7

Table 1: Transition rates for ^6Li . The rate for $3P_{3/2} \rightarrow 2S_{1/2}$ assumes a direct decay; divided by 2π and get $\gamma = 180$ kHz. Numbers obtained from NIST

In order to figure out the linewidth for the $2s \rightarrow 3p$ transition used for cooling, one must also consider the alternative decay paths because of the intermediate energy levels. In addition to the decay path directly from $3P_{3/2} \rightarrow 2S_{1/2}$, there are also the paths

$$3P_{3/2} \rightarrow 3S_{1/2} \rightarrow 2P_{3/2} \rightarrow 2S_{1/2} \quad (65)$$

and

$$3S_{3/2} \rightarrow 3S_{1/2} \rightarrow 2P_{1/2} \rightarrow 2S_{1/2} \quad (66)$$

as shown in the above Figure. The transition rate Γ , decay time τ , and linewidth γ (in Hz) are all related by

$$\frac{1}{\tau} = \Gamma = 2\pi \times \gamma. \quad (67)$$

When there are two possible decay paths in a transition, one adds the corresponding rates Γ for each transition. However, when there is one possible decay path, one must add the decay times τ for each transition. Transition rates are presented in Table (1); numbers were obtained from NIST^{28,29,30}. For the $2P_{1/2} \rightarrow 2S_{1/2}$, the linewidth is $\Gamma \sim 2\pi \times 6$ MHz. In contrast, after considering all the possible decay paths, the linewidth for the $3P_{3/2} \rightarrow 2S_{1/2}$ is $\Gamma \sim 2\pi \times 780$ kHz. The characteristic temperatures for ^6Li are summarized in Table (2).

²⁸ Ralchenko et. al. Nist atomic spectra database. <http://physics.nist.gov/asd3>, 2010

²⁹ A. Filippov. *Z. Phys.*, 69:526, 1931

³⁰ A. W. Weiss. *Astrophys. J.*, page 138, 1963

Characteristic T	$2s - 2s$	$2s - 3p$
Doppler T_D	$140\ \mu\text{K}$	$17\ \mu\text{K}$
Recoil T_R	$3\ \mu\text{K}$	$15\ \mu\text{K}$

Table 2: Temperature limits on the cooling of ^6Li .

Laser frequency stabilization

Introduction

Stabilizing the frequency of the laser to the $2s - 3p$ transition in ${}^6\text{Li}$ allows for cooling to the Doppler-limited temperature of $T_D \approx 20 \mu\text{K}$. In our experiment, an external-cavity diode laser (ECDL) provides narrow linewidth laser light. A typical ECDL consists of a semiconductor laser diode chip which typically has one end anti-reflection coated and an external collimating lens and mirror to complete the resonator. Changing the bandgap of the semiconductor in the diode laser allows for broad tuning of the wavelength. In contrast, small changes in current that power the diode lead to small changes in the temperature of the semiconductor inside the diode laser. Additional changes in frequency come from changes in the refractive index of the semiconductor. The frequency of the laser can be restricted to a narrow band using external optical elements such as gratings, etalons, and cavities restrict the frequency of the laser to a narrow interval. In the ${}^6\text{Li}$ cooling experiment, a DC voltage controls a piezo-electric transducer that changes the length of the laser cavity. A Fabry-Pérot cavity provides additional control over tuning the laser frequency. However, the central frequency of the laser will drift because of external perturbations such as changes in air pressure and temperature. To reduce such drift, a series of feedback loops continuously corrects the laser's frequency. The feedback signal for the $2s - 3p$ transition comes from the technique of saturation absorption spectroscopy, which generates a DC error signal with a zero crossing at the desired central frequency.

Saturated Absorption Spectroscopy

The technique of saturated absorption spectroscopy eliminates the Doppler broadening of observed linewidths in atomic spectra. Collisional, pressure, and power broadening serve as additional mechanisms that increase the observed linewidths. Doppler-broadened linewidths are typically larger than 500 MHz, which sets a rough limit on the resolution of optical spectroscopy. Spectra free of Doppler broadening

effects exhibit much greater sharpness and resolution compared to the Doppler-broadened spectra. Small atomic and molecular interactions hidden by Doppler-broadening have been observed using Doppler-free spectroscopy.

At room temperature, Doppler-broadening typically provides the largest contribution to linewidth broadening. Suppose we have a light source that produces radiation with angular frequency ω in the lab frame of reference, shining on both sides of an atomic sample as shown in Figure (15). For an atom moving at velocity \mathbf{v} , the observed angular frequency seen in the atom's moving frame of reference will be Doppler-shifted. In the atom's frame of reference, the observed radiation from the left will have the shifted frequency

$$\omega_L = \omega - \mathbf{k} \cdot \mathbf{v} \quad (68)$$

and similarly for the radiation coming from the right.

For simplicity, suppose the atom only moves in one dimension so that $\mathbf{k} \cdot \mathbf{v} = kv$. We also assume the atom at rest absorbs radiation at the resonant frequency ω_0 . When the atom moves at velocity v , it absorbs radiation under the condition $\Delta\omega = \omega - \omega_0 = kv$. In other words, an atom moving towards a light source observes light to be upshifted in frequency. For absorption to occur, the frequency of the light source must be downshifted to match the resonant frequency of the atom. The magnitude of the required shift is

$$\Delta\omega = \omega_0 \frac{v}{c} \quad (69)$$

For an ideal gaseous sample of atoms, the number of atoms $N(v)dv$ within some velocity interval v and $v + dv$ follows a Maxwellian distribution given by

$$\begin{aligned} D(v)dv &= \sqrt{\frac{M}{2\pi k_B T}} \exp\left(-\frac{Mv^2}{2k_B T}\right) dv \\ &= \frac{1}{u\sqrt{\pi}} \exp\left(-\frac{v^2}{u^2}\right) dv \end{aligned}$$

where the most probable speed for the atoms is $u = \sqrt{2k_B T/M}$. Putting $v = \Delta\omega/\omega_0 c$ into the above relation gives an absorption with a Gaussian-shaped absorption function

$$g_D(\omega) \propto \exp\left[-\frac{c^2}{u^2} \left(\frac{\Delta\omega}{\omega_0}\right)^2\right] \quad (70)$$

Demanding the above function be normalized by the condition

$$\int_{-\infty}^{+\infty} g_D(\omega)d\omega = 1 \quad (71)$$

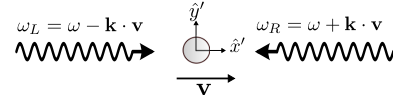


Figure 15: Doppler shift of light observed by a moving atom. A light source provides incident radiation of angular frequency ω in the lab frame. The atom travels at velocity v relative to the lab frame and observes Doppler-shifted light from the left and the right.

gives us the normalizing factor $c/u\omega_0\sqrt{\pi}$ where c is the speed of light. The maximum value of g_D occurs at $\omega = \omega_0$. The function drops to half its maximum value at

$$\Delta\omega_{1/2} = \frac{u\omega_0}{c}\sqrt{\log(2)} \quad (72)$$

The full width at half maximum () is defined as $\Delta\omega_D = 2\Delta\omega_{1/2}$ which gives us

$$\frac{\Delta\omega_D}{\omega_0} = 2\sqrt{\log(2)}\frac{u}{c} \approx 1.7\frac{u}{c}. \quad (73)$$

In terms of frequency f (in units of Hz), the of the Doppler-broadened spectral profile is

$$\Delta f_D \approx 7.16\sqrt{\frac{T}{M}} \times 10^{-7} \times f_0 \quad (74)$$

For ${}^6\text{Li}$, the atomic mass is $M = 6.015$ amu, so the most probable speed is $u = 846.435$ m/s. Thus, we find $\Delta f_D/f_0 \sim 5 \times 10^{-6}$. Thus, for the $2s - 2p$ transition (671 nm), we expect Doppler broadening of 2.14 GHz and for $2s - 3p$ transition (323 nm), the Doppler broadening is 4.5 GHz.

One method of obtaining Doppler-free signals is by saturated absorption spectroscopy. For simplicity, consider a two state system with a ground state $|g\rangle$ and excited state $|e\rangle$. Let the number density of atoms in the ground and excited states be $N_g(v)$ and $N_e(v)$, respectively. In saturated absorption spectroscopy, a laser provides monochromatic light at the angular frequency ω . A beam splitter then divides the beam into a pump and probe. Deriving the two beams from a single source ensures they have the same frequency. The power of the probe beam is typically 10-20% of the stronger pump beam. The two beams then go into opposite ends of a container with the atomic sample, which is heated to produce atomic vapor. A simple schematic is shown in Figure (16).

Atoms in $|g\rangle$ that have velocity $v = (\omega - \omega_0)/k$ interact with the pump beam. Many of the atoms will get excited to $|e\rangle$, so there will be few atoms remaining in $|g\rangle$ to absorb laser light from the probe beam. This process is referred to as *burning*, where the hole burnt in $|g\rangle$ is equal to the power-broadened homogeneous linewidth given by

$$\Delta\omega = \Gamma\sqrt{1 + I/I_{sat}} \quad (75)$$

where Γ is the natural linewidth of the transition, I is the beam intensity, and I_{sat} is the saturation intensity. See Figure (17).

To perform spectroscopy, the transmission of the probe beam through the atomic sample is recorded as the frequency of the laser varies. When $|\omega - \omega_0| \gg \omega$, the laser is far off resonance so the pump and

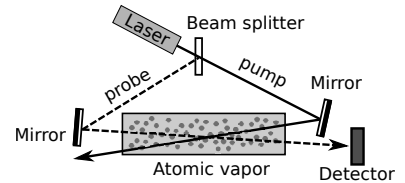


Figure 16: A cartoon of a saturated absorption spectroscopy experiment. A beam splitter divides a beam into a pump and probe, both with the same frequency. The probe beam is typically 10% of the intensity of the pump beam. Both beams intersect inside the vapor cell containing the atomic sample. A photodetector detects the transmission of the probe through the atomic sample.

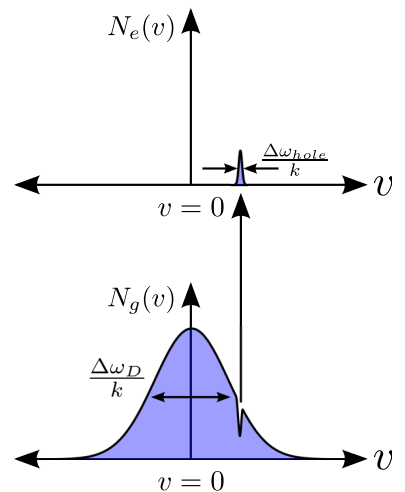


Figure 17: Hole burning caused by the laser beam. For a given laser frequency, the beam interacts with the atoms in the corresponding velocity group. The atoms are excited into $|e\rangle$ so there is a decrease in the number of atoms in $|g\rangle$. The pump beam creates a bigger than the one created by the probe beam.

probe beams interact with different velocity groups. Close to resonance, we have $\omega \approx \omega_0$ so both beams interact same velocity group of atoms $v \approx 0$. The pump beam proceeds to depopulate $|g\rangle$ by burning. There are few atoms in $|g\rangle$ to interact with the probe beam because the population density difference $N_e - N_g$ approaches zero, as shown in Figure 18. Hyperfine splitting of ${}^6\text{Li}$ shown in Figure 14.

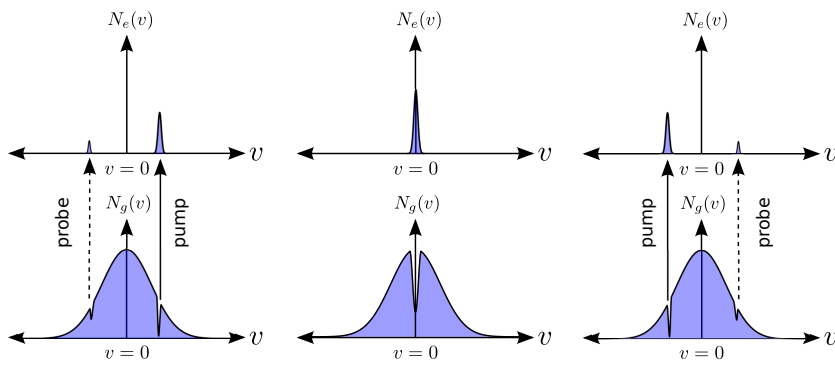


Figure 18: Population densities in $|g\rangle$ and $|e\rangle$ with pump and probe beams. The pump creates a bigger than the probe. The effect of the pump and probe beams is shown for three different laser frequencies: below, about equal to, and above the atomic resonance, respectively.

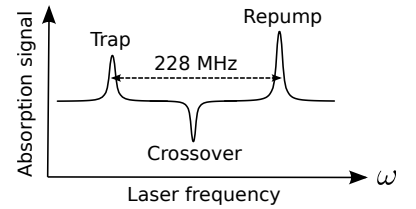


Figure 19: Cartoon of the absorption signal for the $2s - 3p$ transition. The hyperfine splitting between the trap ($F = 3/2$) and repump ($F = 1/2$) is 228 MHz. The center dip is called the crossover and is an artifact of the experiment. The crossover comes from the interaction of the pump and probe beams when there are two nearby hyperfine splittings. In short, the burning by one transition reduces the absorption for another transition, resulting in a peak directly between the two hyperfine states. The crossover is actually helpful to us because it can serve as a reference to aid in locating the other trap and repump transitions.

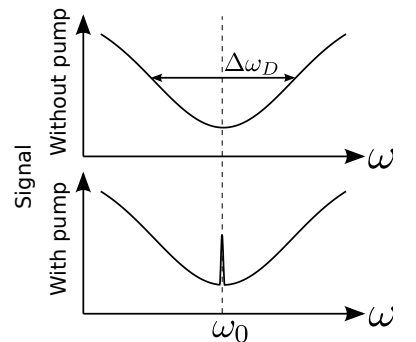


Figure 20: Doppler-broadened and Doppler-free absorption signals. Without the pump beam, the probe interacts with the atomic sample yielding only a Doppler-broadened spectrum. With the pump beam, when the laser frequency is at the atomic resonance, the pump beam burns a in a ground state. Thus, there are few atoms for the probe to interact with and one observes a sharp peak centered at the atomic resonance.

Lock-in detection

The detector measures the weak probe beam transmitted through the heatpipe. We use a lock-in amplifier to increase the signal strength and also generate an error signal. The signal produced by the lock-in is proportional to the first derivative of the absorption curve. The error signal produced by the lock-in is a suitable feedback signal because of the zero at atomic transition frequency.

A lock-in amplifier recovers a signal buried in noise. The frequency of the laser modulated at ω_m scans the Doppler-free spectrum centered at ω_0 . A photodiode detects the modulated absorption signal and sends the signal into the lock-in amplifier. The original modulation signal ω_m is also sent into the lock-in amplifier where an arbitrary phase ϕ is added. The lock-in then multiplies the two signals together. A low-pass filter removes the oscillatory components, producing an error signal.

To see how error signal arises explicitly, let the modulated laser

frequency be given by

$$\omega_L = \omega_c + A_m \cos(\omega_m t) \quad (76)$$

where ω_c is the central frequency of the laser. Assume that the drifts of the central laser frequency are much slower than the period of the frequency modulation, thus $\omega_c \ll \omega_m$. Let the absorption signal be $S(\omega_L)$. Make the amplitude of the absorption signal A_m sufficiently small so that $S(\omega_L)$ can be approximated as a Taylor series about ω_c . Doing so

$$S(\omega_L) = S(\omega_c) + S'(\omega_c)(\omega_L - \omega_c) + O((\omega_L - \omega_c)^2) \quad (77)$$

From Equation (76) and after dropping higher order terms, the signal becomes

$$S(\omega_L) = S(\omega_c) + S'(\omega_c)A_m \cos(\omega_m t) \quad (78)$$

Now pass the reference modulation signal through a mixer to give it a phase-shift ϕ and amplitude A_r . The lock-in amplifier then multiplies, or *mixes*, the two signals together to give

$$\begin{aligned} M(\omega_L) &= S(\omega_L) \times A_r \cos(\omega_m t + \phi) \\ &= [S(\omega_c) + S'(\omega_c)A_m \cos(\omega_m t)] A_r \cos(\omega_m t + \phi) \\ &= SA_r \cos(\omega_m t + \phi) + S' A_m A_r \cos(\omega_m t) \cos(\omega_m t + \phi) \end{aligned}$$

Using the trig identity $\cos \theta \cos \phi = \frac{1}{2} [\cos(\theta - \phi) + \cos(\theta + \phi)]$ we finally get

$$\begin{aligned} M(\omega_L) &= SA_r \cos(\omega_m t + \phi) + \frac{1}{2} S' A_m A_r \cos(2\omega_m t + \phi) \\ &\quad + \frac{1}{2} S' A_m A_r \cos(\phi) \end{aligned} \quad (79)$$

Putting the mixed signal M through a low-pass filter to first order removes all the oscillatory terms. Thus, we get an error signal

$$E(\omega_L) = \frac{1}{2} S' A_m A_r \cos(\phi) \quad (80)$$

The error signal has three important properties:

1. Explicit dependence on the phase ϕ
2. Proportional to first derivative of the signal S
3. Proportional to modulation amplitude A_m

Assuming Doppler-broadening (inhomogeneous broadening), the lineshape function g_D is given by equation (70). Taking the first derivative, we get the error signal

$$E_D(\omega) \propto -\frac{2c^2}{\omega_0^2 u^2} (\omega - \omega_0) \exp \left[-\frac{c^2}{u^2} \left(\frac{\Delta\omega}{\omega_0} \right)^2 \right] \quad (81)$$

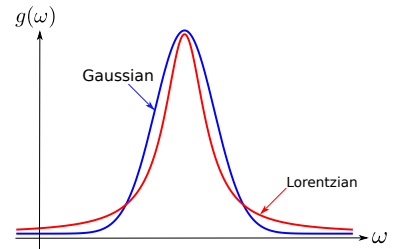


Figure 21: Plot of Gaussian and Lorentzian lineshape functions. Notice that the Gaussian bell shape falls off more rapidly than the Lorentzian.

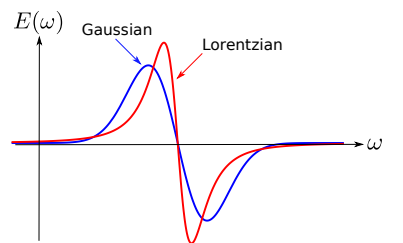


Figure 22: Plot of the error signals for Gaussian and Lorentzian signals. The **zero-crossing** is the point at which the curves intersect the x axis.

where $\Delta\omega = \omega - \omega_0$.

Similarly, if we assume only homogeneous broadening, the line-shape function is a Lorentzian g_L . Taking the first derivative gives us the error signal

$$E(\omega) \propto -\gamma \times \frac{(\omega - \omega_0)}{[4\pi^2(\omega - \omega_0)^2 + (\gamma\pi)^2]^2} \quad (82)$$

where γ is the linewidth of the transition. A plot of the lineshapes is shown in Figure (21) and a plot of the error signals is shown in Figure (22).

Feedback into laser

The absolute laser frequency stabilizes to the Doppler-free signal from the $2s - 3p$ transition. The laser frequency is carefully tuned to the zero-crossing of the error signal. The zero-crossing occurs at the resonant frequency of the $2s - 3p$ transition, as seen in Figure (23). As the laser frequency drifts, the error provides continuous adjustment to the laser's frequency.

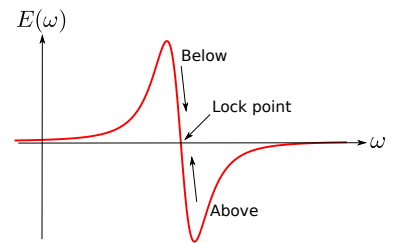


Figure 23: Plot of error signal. This signal provides feedback to the laser. If the laser frequency is below the atomic resonance (the **lock point**), then the error signal will provide feedback to the laser and increase its frequency. However, if the laser frequency is above the atomic resonance, the feedback will cause the laser to decrease its frequency.

Experiment

The major components of our home-built laser frequency stabilization system are the modulation circuit, the demodulation circuit (i.e. lock-in amplifier), the photodiode amplifier, the acousto-optic modulator (AOM), and the saturation absorption spectroscopy optical setup. The basic idea is that the technique of saturation absorption spectroscopy produces a reference signal that is picked out by the lock-in amplifier. A feedback circuit then sends an error signal back into the laser to lock the frequency of the laser to an atomic transition. The modulation and lock-in circuits were built using inexpensive off-the-shelf analog components based on Sowka³¹.

Modulation circuit

The modulation circuit provides a reference signal for the lock-in amplifier and also a signal that controls the voltage-controlled oscillator (VCO) driving the acousto-optic modulator (AOM). For our experiment, the modulation frequency f_m is at 50 kHz. Because the operating voltage range of the VCO is 1 to 16 V, the original modulation signal is added to a DC offset generated by a computer. The VCO provides linear tuning at 4.5 MHz/V with a center frequency of 67 MHz and a bandwidth of 52 to 98 MHz. Thus, for a linewidth of $\gamma \approx 700$ kHz, the corresponding output voltage of the VCO is $1\text{ V}/4.5\text{ MHz} \times 700\text{ kHz} \approx 150\text{ mV}$.

The heart of the modulation circuit is the XR-2206 monolithic function generator integrated circuit (IC). This chip has the capability to produce sine, square, triangle, ramp, and pulse waveforms. Because only a sine wave is required for the lock-in amplifier, a sine wave generation circuit was constructed as shown in the schematics (see Appendix). Simple modifications of the circuit allow for the output of the other waveforms (see the data sheet).

The IC is operated by a split-supply. The input cable has +15V, ground, -15V, and +24. The +15V, ground, -15V are fed into filter capacitors and inductors to help reduce noise from the power supply. A pair of regulators provide a stable +12V and -12V. There is an addi-

³¹ J. Dalibard. A home-built lock-in amplifier for laser frequency stabilization. *Can. J. Phys.*, 83:907–918, 2005

tional regulator used to provide a stable +17V output.

The output frequency of the chip is determined by the external timing capacitor across pins 5 and 6 and variable resistor from pin 7 to -12V. The oscillation frequency is given by

$$f_0 = \frac{1}{RC} \text{ Hz.} \quad (83)$$

The capacitor was set at the minimum value of 1 nF. Lower values were tested, but the output waveform was heavily distorted. A 100 kOhm potentiometer adjusts the output frequency f_0 . A 5 K resistor is in series with the potentiometer to give a theoretical maximum operating frequency of 200 kHz. The measured bandwidth was about 10 kHz $< f_0 < 185$ kHz. As the frequency increases, the amplitude of the waveform must be reduced to avoid distortions of the sine wave.

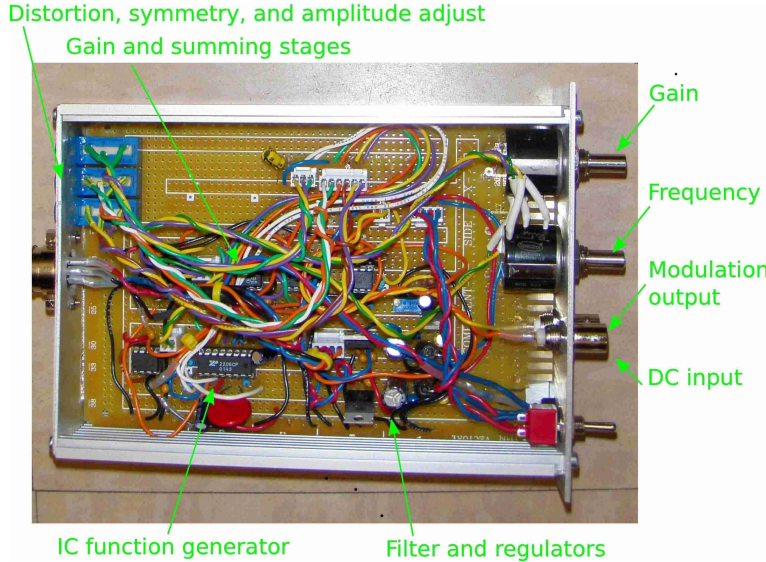
To reduce the distortion of the sine wave, the harmonic content of the output can be adjusted. The potentiometer across pins 15 and 16 adjust the symmetry of the waveform. In addition, the potentiometer across 13 and 14 provides fine adjustment for the shape of the waveform. The potentiometer at pin 3 affects the amplitude of the waveform. The circuit was originally constructed to output a triangle wave because the sine wave was heavily distorted. However, by reducing the amplitude and adjusting the waveform symmetry, it is possible to obtain a sine wave with minimal distortions.

The output of the IC gets passed to an inverting amplifier. For an input resistor R_{in} and feedback resistor R_f , the gain of the inverting amplifier is given by

$$G_V = \left| \frac{V_{out}}{V_{in}} \right| = -R_f/R_{in} \quad (84)$$

where V_{out} and V_{in} are the input and output voltages, respectively. For $R_{in} = 5$ K and $R_f = 10$ K (adjustable), the gain is $G_V = 2$.

After the inverting amplifier, a DC signal is added to the modulation signal. The DC signal is provided by a computer and first sent into a follower, which is simply just a non-inverting amplifier with unity gain. Its purpose is to provide a high input and low out impedance thereby providing effective isolation of the output signal from the signal source. The follower ensures little current is drawn from the source so that any adverse loading problems can be avoided. After the follower, a summing circuit combines the modulation signal with the DC offset. An inverting amplifier of unitary gain is placed after the summing circuit to make the waveform positive again.



Demodulation circuit

The demodulation circuit generates the first derivative of the absorption signal. Key elements of the demodulation circuit are the phase shifter, RF mixer, and low-pass filter. The reference signal from the modulator is AC coupled to a phase shifter and then mixed with the absorption signal. The output of the mixer is sent through a low-pass filter to eliminate the AC components. The end result is the first derivative of the absorption signal, called the *error signal*.

To eliminate the DC offset generated by the modulation circuit, a high-pass filter AC couples the modulation signal to the input of the phase shifter. Values chosen were $R = 100$ Ohms and $C = 100$ nF, giving a -3 dB breakpoint of about 16 kHz.

The phase shifter creates a phase difference between the modulation signal and the absorption signal. A phase shifter as shown in Figure () was designed to operate at an angular frequency of ω . The voltages at the inputs V_+ and V_- are given by

$$V_+ = V_{in} \frac{i\omega RC}{1 + i\omega RC} \quad \text{and} \quad V_- = \frac{1}{2} (V_{in} + V_{out}) \quad (85)$$

where V_{in} and V_{out} are the input and output signals, respectively. Because the op-amp equalizes its inputs, we can set $V_+ = V_-$ and obtain

$$\frac{V_{in}}{V_{out}} = \frac{1 - i\omega RC}{1 + i\omega RC} \quad (86)$$

Let the phase shift be ϕ so that we can re-write the above equation as

$$\tan(\phi) = \frac{-2\omega RC}{1 - (\omega RC)^2} \quad (87)$$

Figure 24: Overhead view of the home-built modulation circuitry. A computer provides a DC input. The output of the circuit is a sine wave with a DC offset. The user can control the frequency and amplitude of the sine wave using the pots on the box. Trim pots on the back allow one to adjust the harmonic content of the sine output. First, adjust "symmetry" so that the wave is centered vertically. Then adjust the "distortion" for further adjustment. The "amplitude" provides additional fine adjustment over the output sine wave.

Using trigonometry, we rewrite the above quantity as

$$\tan(\phi/2) = \frac{1}{RC\omega}. \quad (88)$$

The phase difference is determined by a variable resistor. For a modulation signal of 50 kHz, a capacitor of $C = 100 \text{ nF}$ and variable resistor of 1 k results in a 90 degree phase shift. A follower was placed before the phase shifter to prevent any adverse loading effects.

The absorption signal first passes through a high-pass filter to eliminate any DC components. If any DC components are present in the absorption signal, then the signal from the output of the mixer will be diminished.

Since the absorption signal contains a significant amount of noise, filtering it before the mixer helps reduce the noise at the output of the lock-in amplifier. High frequency and $1/f$ noise are removed by using a bandpass filter centered at 50 kHz. To eliminate as much noise as possible, the bandpass filter needs to have steep rolloffs into the stopbands. The order of a filter determines how steep the rolloff is into the stopband. For example, a simple first-order RC filter has a rolloff of 6 dB/octave. *Passive filters* are made from passive elements, usually resistors, capacitors, inductors, and transforms. Passive filters do not require any external power source. Higher-order filter types such as Butterworth, Chebyshev, and Bessel filters make it possible to create filters with steep rolloffs. The main disadvantage of passive filters is their use of inductors, which are typically bulky and lossy. To avoid these problems, one uses active filters that have the characteristics of ideal RLC filters.

An *active filter* uses amplifiers such as op-amps to create RLC filters without using inductors. Cascading active filters allows one to create higher-order filters. A relatively simple implementation of an active filter is the *voltage-controlled voltage-source* (VCVS) filter. Only a small number of parts are required and gain is achieved by using a non-inverting amplifier as part of the filter. The -3 dB cutoff frequency f_c is set by R and C given by

$$f_c = \frac{1}{2\pi RC}. \quad (89)$$

A VCVS bandpass filter with a center frequency at 50 kHz was made by cascading together a low and high-pass filter. The frequency response of the fabricated filter is shown in Figure (). Because the $1/f$ noise is dominate at the lower frequencies, two low-pass filters were cascaded together resulting in a 4th-order filter. A single high-pass filter eliminates high-frequency noise. The filters mimic the response of a Butterworth filter, which has maximum flatness in the passband. A non-inverting amplifier amplifies the filtered absorption signal.

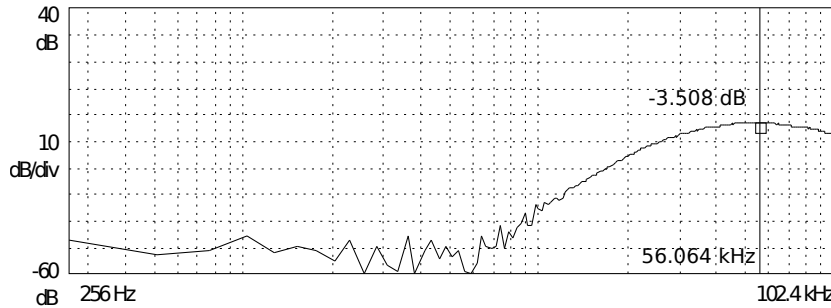


Figure 25: Lock-in band pass filter made up of active low and high-pass filters. The active low-pass filter has 2 poles with a -3 dB point at about 55 kHz. The active high-pass filter has two poles with a -3 dB point at about 30 kHz.

An RF mixer multiplies the filtered absorption signal with the phase-shifted modulation signal. The mixer has two inputs and one output. The local oscillator (LO) and the radio frequency (RF) signals are mixed together to produce an intermediate frequency (IF). Choosing the proper mixer is crucial to getting the demodulator working³². Under-specifying the specifications will yield marginal performance, but over-specification means you will pay for extra for unnecessary performance characteristics. There are four basic guidelines with choosing a mixer:

- 1 Determine if the mixer needs to be surface mounted or not.
- 2 Get a rough estimate of the drive power in dBm for the LO.
- 3 Figure out what the required frequency range is for the application.
- 4 If necessary, some applications might specify the acceptable amount of total harmonic distortion caused by mixing the LO and RF signals.

For the demodulation circuit, we demand that the LO and RF inputs operate over the frequency range 50-200 kHz. Assuming an input impedance of 50 ohms and a pk-pk voltage of 0.5 V, the corresponding input power is 7 dBm. To first-order for diode mixers, the LO power should be 10 dB greater than the highest anticipated input signal level. The RF input power must be lower than the 1 dB compression point, which is the high end of a mixer's linear range. Given these conditions, a level 7 mixer from Mini-circuits (SRA-6+) was chosen with a bandwidth of 3 kHz - 100 MHz.

The output of the RF mixer is sent to a low-pass filter to eliminate the AC components. As a first test, a 4th-order passive Butterworth low-pass filter was constructed and placed at the DC output of the lock-in. High frequency components were removed resulting in a reasonable signal-to-noise ratio (SNR). However, the measured risetime of the lock-in was about 200 ms, which is the same as the risetime for the commercial lock-in. Because the signal from the lock-in amplifier gets fed back into the laser, fast rise times at the order of 1 ms are

³² Mini-Circuits. How to select a mixer, June 2008

required. The passive Butterworth filter was replaced with an active 2nd-order Butterworth low-pass filter with a cutoff frequency of about 200 Hz. The measured risetime of the lock-in amplifier was about 3 ms. Removing the AC components of the mixed signal resulted in a low-noise DC signal at the output of the lock-in amplifier.

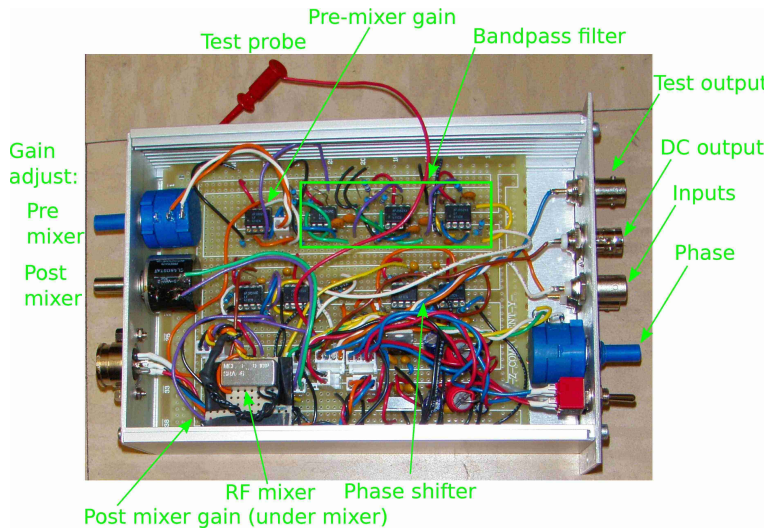


Figure 26: Overhead view of the home-built lock-in amplifier circuitry. There are two ac-coupled inputs and one DC output. The input modulation signal provides a reference for the lock-in. A pot on the front provides phase adjustment of the input modulation signal. There is also an input for the unfiltered absorption signal. The DC output of the lock-in amplifier is proportional to the phase difference between the modulation and absorption signal. There are pots on the back of the box to provide control of the gain of the lock-in amplifier. The “pre-mixer gain” affects the absorption signal before the mixer. The “post-mixer” affects the DC signal after the low-pass filter. There is also a test probe with an output for debugging purposes.

Photodiode amplifier

A photodiode converts a light signal at a sufficient wavelength into an electrical signal. An equivalent circuit of the photodiode is shown in Figure (27). Because of the PN junction, the photodiode has a capacitance C_{ph} .

The photodiode has two modes of operation. The *photovoltaic* mode occurs when there is zero bias voltage across the PN junction. The flow of any current is restricted and voltage builds up across the PN junction. In contrast, the *photoconductive* mode occurs when the PN junction is reversed biased. Because of the reverse bias, the width of the depletion layer increases thereby decreasing the capacitance of the PN junction. The decrease in capacitance means a significant increase in response time of the photodiode. However, as the response time is increased, the photodiode also exhibits more electronic noise.

For our experiment, we operate in the photoconductive regime for fast response times. Because the photocurrent is at the order of microamperes and below, it is necessary to use a current to voltage amplifier. The simplest way to obtain a voltage is to use a large ($> 1\text{M}\Omega$) resistor R_L in series with the photodiode. The large resistor gives a large time constant of $R_L \times C_{ph}$ and also added noise onto the signal.

The solution is to connect the photodiode to the virtual ground of a

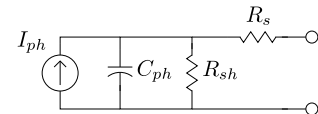


Figure 27: Equivalent circuit of a photodiode. An ideal current source I_{ph} is in parallel with a shunting capacitance C_{ph} due to the depletion region. There is also a series resistance of R_{sh} , typically at least $10\text{ M}\Omega$ and higher. Contact resistance and resistance of the undepleted silicon are both represented by R_s , normally under $100\ \Omega$.

Gain and offset

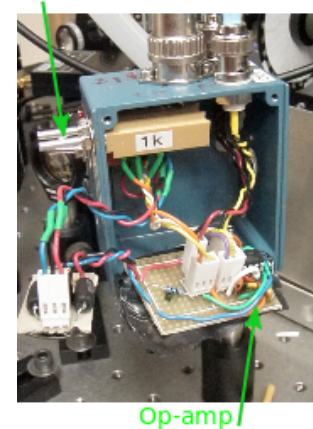


Figure 28: Picture of the transimpedance amplifier for the photodiode.

transimpedance amplifier. A feedback resistor R_f is connected across the output and the virtual ground. To compensate for the capacitance of the photodiode, a capacitor C_f is added in parallel to R_f . The capacitance is given by

$$C_f = \sqrt{\frac{C_{in}}{2\sqrt{2}\pi f_{GBW}R_f}} \quad (90)$$

where f_{GBW} is the gain bandwidth frequency and $C_{in} = C_{cm} + C_{ph}$ for a common mode input capacitance C_{cm} of the op-amp. Large values (> 1 MHz) of f_{GBW} are desirable to reduce the rise time. The trade off is that the smaller values of C_f cause ringing in the circuit as shown in Figure (29(a)).

The transimpedance amplifier was tested by using a 671 nm laser beam (about 5 mW) and a Thorlabs DET36A photodiode. A function generator produced a transistor-transistor logic (TTL) signal that drove the AOM. If the state of the pulse was 5V, then the beam would be diffracted towards the photodiode. For a state of 0V, the beam would not hit the photodiode.

The purpose of the test was to determine if the transimpedance amplifier could respond to a 50 kHz signal with minimal distortion and fast risetimes. The capacitance of the photodiode was found to be about $C_{ph} = 40$ pF. The transimpedance amplifier had an AD 829 op-amp with a gain band width product of $f_{GBW} = 600$ MHz and a common-mode capacitance of $C_{cm} = 1.5$ pF. Thus $C_{in} = 41.5$ pF and so it was expected $C_f \approx 0.3$ pF. However, to eliminate the ringing, the value of C_f was increased to about 4 pF. The ringing was caused by the diode's capacitive nature on the inverting input of the op-amp. Increasing the value of C_f reduced the ringing. The risetime was found to be about 1 μ s with a 50 kHz squarewave input.

With an AD 797 op-amp, the risetime was found to be 280 ns. The slew rate for the AD 797 is $20V/\mu s$ resulting in an expected 250 ns risetime for a 0 to 5V pulse. Although the AD 797 has a very fast rise time, it turns out that the AD 829 removes the ringing as well as having a decent rise time.

Acousto-optic modulator (AOM)

An acousto-optic modulator uses sound waves to diffract a beam of light along with shifting the beam's frequency and changing its intensity. The diffracted beam emerges from the AOM at an angle θ given by

$$\sin \theta = \frac{m\lambda}{2\Lambda} \quad (91)$$

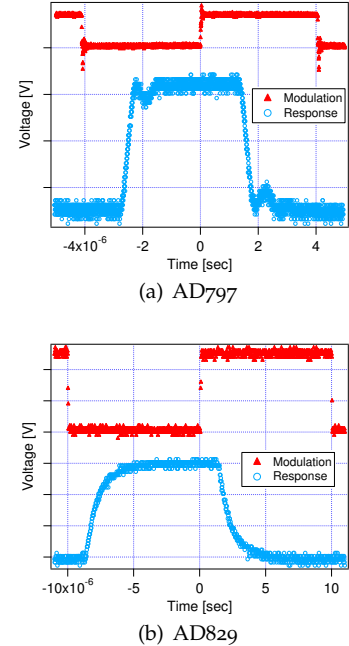


Figure 29: Response of transimpedance amplifier. A 50 kHz TTL signal turn on and off a laser beam focused on a photodetector. The output of the photodetector was sent into an oscilloscope. Graphs are shown with arbitrary vertical offsets. (a) For the AD797, the risetime was about 280 ns, although some ringing was present. (b) For the AD829, the ringing was eliminated, although the risetimes were 1.2 μ sec.

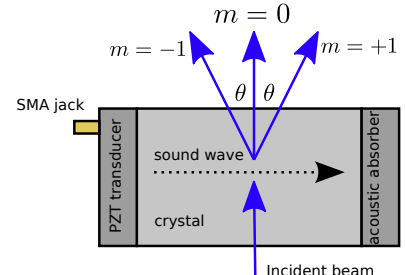


Figure 30: Cartoon of the AOM. An RF source drives a piezo-electric transducer (PZT). The PZT creates sound waves that propagate through a crystal (in a direction away from the SMA jack). An incident beam passes through the crystal and is diffracted. Only the first and zeroth orders are shown. The AOM can change the frequency of the light by coupling the photons with the phonons in the crystal inside the AOM.

where λ is the wavelength of light, Λ is the wavelength of sound in the crystal of the AOM, and the diffraction order m is an integer. The light scatters from moving planes, so a beam of frequency f_0 and order m will be shifted by an amount

$$f = f_0 + m\Lambda. \quad (92)$$

The sound waves are produced in a crystal from an RF source connected to a voltage-controlled oscillator (VCO). The home-built modulation circuit provides a modulation signal to the VCO. Figure (31) shows the calibration of the VCO.

The AOM uses a double-pass configuration to eliminate the effect of the beam getting deflected back and forth as the RF signal is varied. The double-pass configuration uses a prism to retro-reflect the m^{th} order of the beam back into the AOM. In our setup, $m = 1$ because there is a large loss in beam power with the higher orders. After a second pass through the AOM, there is a frequency offset of $2m\Delta\omega$ where $\Delta\omega$ is the change in angular frequency due to the first pass through the AOM.

The efficiency of the AOM was measured to minimize the reduction in the beam power. First, the beam power P_0 was measured with the AOM off in the single-pass configuration. Then, the 1st order beam power was measured with the AOM on. The *single-pass efficiency* is defined as $\epsilon_{\text{single}} = P_1/P_0$. Similarly, the AOM *double-pass efficiency* is defined as $\epsilon_{\text{double}} = P'_1/P'_0$ where the prime indicates the measured powers after two passes through the AOM. The *overall AOM efficiency* is defined to be $\epsilon_{\text{overall}} = P'_1/P_0$. See Table (3) for results.

Saturated Absorption Spectroscopy setup

Using saturated absorption spectroscopy, we measured the Doppler-free spectra for the $2S_{1/2} \rightarrow 3P_{3/2}$ transition in ${}^6\text{Li}$. A heat pipe oven produced ${}^6\text{Li}$ vapor at about 380 – 390 deg C and roughly 6 mtorr. The heat pipe had to be pumped, heated, cooled, and re-pumped multiple times to be at sufficient operating conditions. Results after a few weeks of pumping are shown in Figure (34).

A second harmonic generation laser produces 646 nm light that is frequency-doubled to 323 nm. The beam first passes through a beam splitter (BS) that sends part of the beam to the atom cooling experiment and the other part of the beam to the Doppler-free setup. A VCO drives an AOM to modulate the center wavelength of a laser. The AOM is setup in a double-pass configuration to eliminate Bragg diffraction, which causes the beam to be deflected back and forth. After the AOM, the beam passes through a beam splitter. Part of the beam (more than 80%) called the **pump** (solid line) passes through a

Configuration	P_{off}	P_{on}	ϵ
Single-pass	4.80	3.95	82%
Double-pass	4.37	2.97	68%

Table 3: Measurements of AOM efficiency. Units are in mW. The overall AOM efficiency was found to be 62%, which is an acceptable value. P_{on} and P_{off} represent beam powers for when the AOM is on and off, respectively.

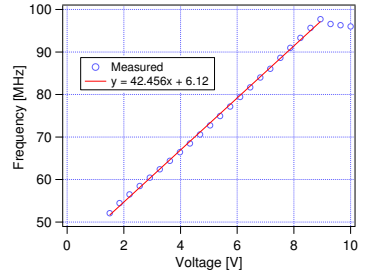


Figure 31: Calibration of the VCO. For a given input voltage from a computer, a BK Precision Model 103 frequency counter (1 MHz to 3 GHz) measured the corresponding output frequency. A linear fit gives a conversion between the voltage and frequency. The fit ignores the last few data points of the non-linear region of the VCO.

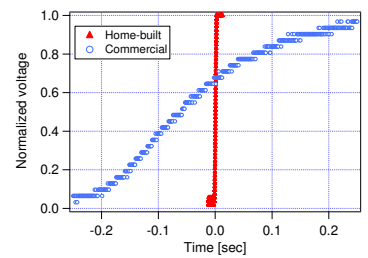


Figure 32: Risetimes of the lock-in amplifiers used to obtain the spectra. We want to show what the rise times were in order to get a decent signal with the old setup (using the commercial lock-in) versus the new setup (using the home-build lock-in). For the commercial lock-in amplifier, the risetime was about 210 msec. For the home-built lock-in amplifier, the risetime was about 2.8 msec. Surely the commercial lock-in can be set to have a faster rise time, however one would not see a signal at all! Thus, it's not so much about the lock-in amplifiers but rather the bandwidth of the entire detection setup in each case.

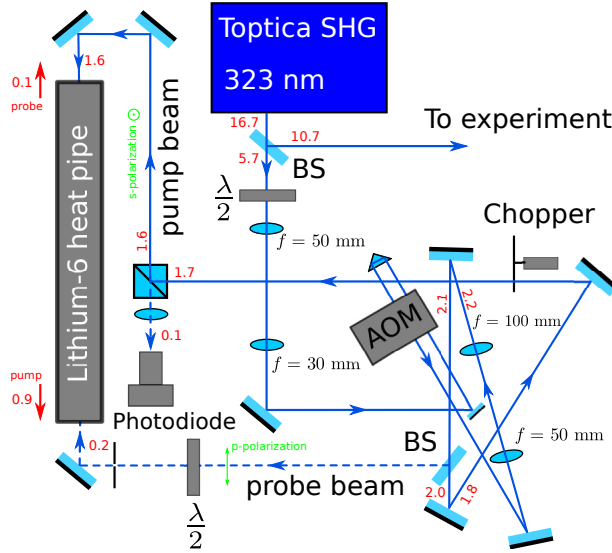


Figure 33: Schematic of the optical setup.

chopper and then into the heatpipe. The remaining part of the beam called the **probe** (dotted line) goes directly to the heat pipe and then into the photodetector. The pump and probe are s and p-polarized, respectively so that we can split the beams up with a cube. The lenses are for the two telescopes used to adjust the beam waist for the AOM. The numbers in red correspond to the measured beam power (in mW) using a UV detector and wavemeter (the higher orders from the AOM were eliminated with an iris).

Measurements were first taken with a commercial lock-in amplifier (*Signal Recovery Model 5105*). A chopper modulated the pump beam at 1.5 kHz. The laser scanned 228 MHz in 8.6 seconds. The optical setup is shown in the above Figure. Doppler-free spectra are shown on the next page. For faster sweeps, RC effects were observed as shown in Figure (35).

The commercial lock-in was then replaced with the home-built modulator and lock-in. The modulator produced a 50 kHz sine wave that drove the AOM. The laser scanned 228 MHz in 0.27 seconds and the resulting spectra are shown on the next page.

Laser stabilization

Having obtained the Doppler-free spectra of ${}^6\text{Li}$, we can now lock the laser to the "trap" transition. A schematic of the laser stabilization system is shown in the Figure on page 49. Laser stabilization system. An External-Cavity Diode Laser (ECDL) provides 646 nm that is split into two beams. One beam goes into a Fabry-Pérot cavity and the other beam goes into a tapered amplifier (TA) to increase the power

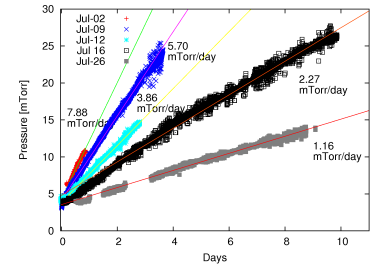


Figure 34: Heatpipe pressure after repumping. The pressure of the heatpipe was monitored after pumping to about 3 mtorr with a vacuum pump. After the first few pumps, the pressure would increase at a higher rate than the pressure increase after the pumping a few weeks later. Data courtesy of Pedro Duarte.

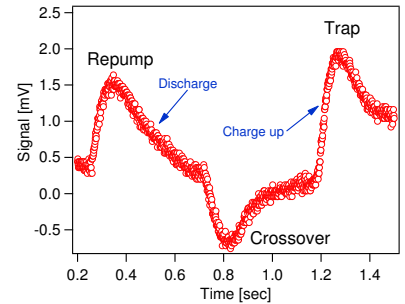


Figure 35: Scope capture of the RC effects in the absorption signal. The commercial lock-in is limited in its bandwidth due to the chopper operating at 1.5 kHz and the low-pass filter ($\tau = 100$ ms) after the mixer in the lock-in. With fast scan times (sweep at 1 Hz) of the laser, one can see clear RC effects due to the low-pass filter in the lock-in amplifier. There were no RC distortions at scan times around 300 mHz.

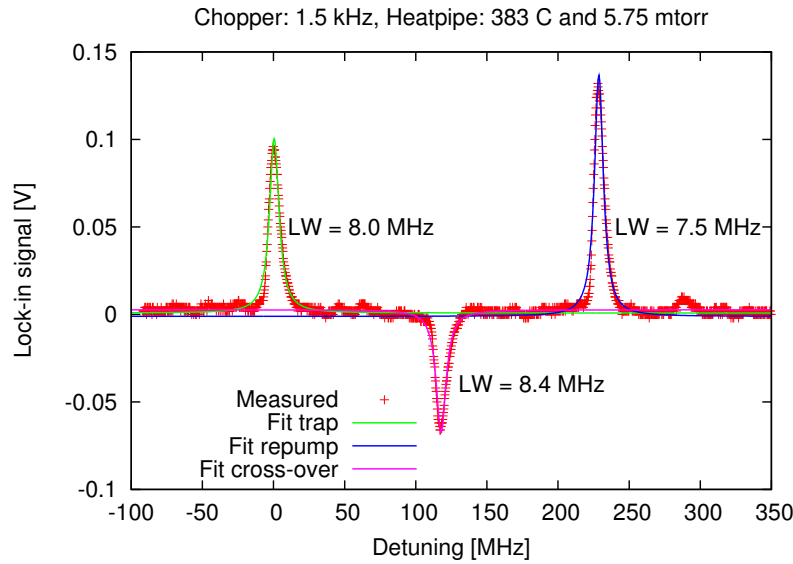


Figure 36: Doppler-free spectrum of ${}^6\text{Li}$ using the commercial lock-in amplifier. The peaks were fit to Lorentzian functions thus giving the transition linewidths. The chopper was set at 1.5 kHz. The heatpipe was approximately at the optimum operating temperature of about 383 deg C and a pressure of 5.75 mtorr. Previously, the laser was locked to the side of trap signal.

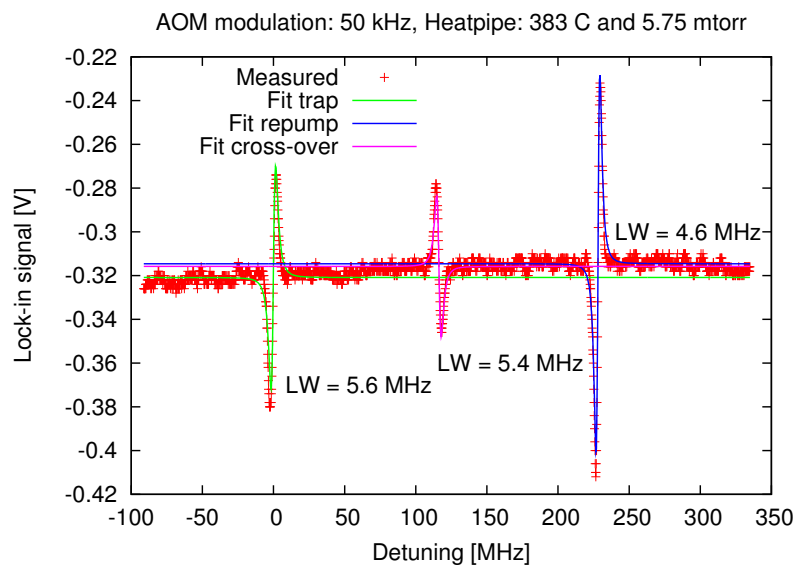
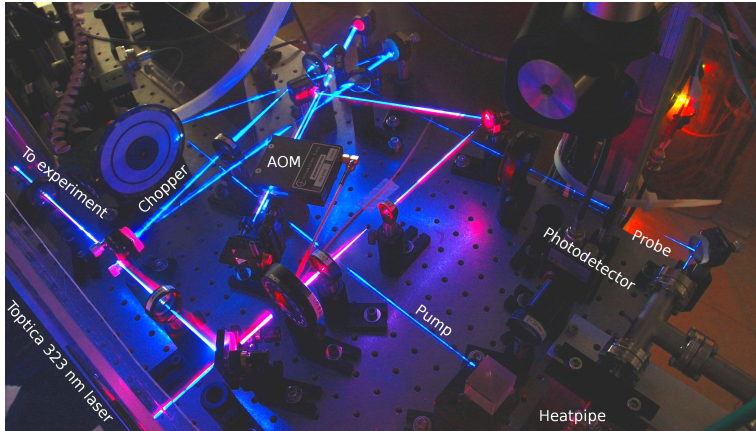


Figure 37: Doppler-free spectrum of ${}^6\text{Li}$ using the home-built lock-in amplifier. The error signals were fit to the first derivative of a Lorentzian to get the transition linewidths. The DC offset is due to the residual intensity modulation of the probe beam by the AOM.



of the beam. A photodetector after the Fabry-Pérot cavity sends an error signal back into the ECDL. After the TA, the beam is sent into a frequency-doubling crystal where the output is 323 nm light.

The beam is split once again, one part goes to the heat pipe and the other goes to the ${}^6\text{Li}$ cooling experiment. The beam going to the heatpipe is first modulated by an AOM and then split into the pump and probe beams. A chopper then modulates the pump beam. The probe beam passes through the heat pipe and a photodetector detects the transmission of light through the heat pipe.

The absorption signal from the photodetector is first sent into the home-built lock-in amplifier. A DC offset from a computer is added to a 50 kHz modulation signal in order to drive the AOM properly. The reference modulation signal (with the DC offset filtered off) is mixed with the absorption signal. After the home-built lock-in, the signal is sent into the commercial lock-in amplifier to eliminate the offset in the absorption signal, which is due to modulating both the pump and the probe beams. The bandwidth of the commercial lock-in is $f = 1/(2\pi 3\text{ ms}) \approx 50\text{ Hz}$. The Doppler-free spectrum for the $2s - 2p$ transition without the DC offset is shown in Figure on the next page.

After the commercial lock-in, the signal is fed into a proportional integral derivative (PID) controller which sends feedback into the Fabry-Pérot cavity. As the laser frequency drifts, the cavity changes its length to compensate for the change in laser frequency.

Figure 38: Long exposure (about 45 sec) of the optical setup. The camera's CCD is not sensitive to the 323 nm light. The beam caused a piece of paper to fluoresce, thus making the beam visible and appear blue. The residual red 646 nm light comes from the Toptica laser. Because the frequency doubling crystal is not perfect, some of the red light will be present in the UV beam. ©2010 Adam Reed, Will Hardy, and Pedro Duarte.

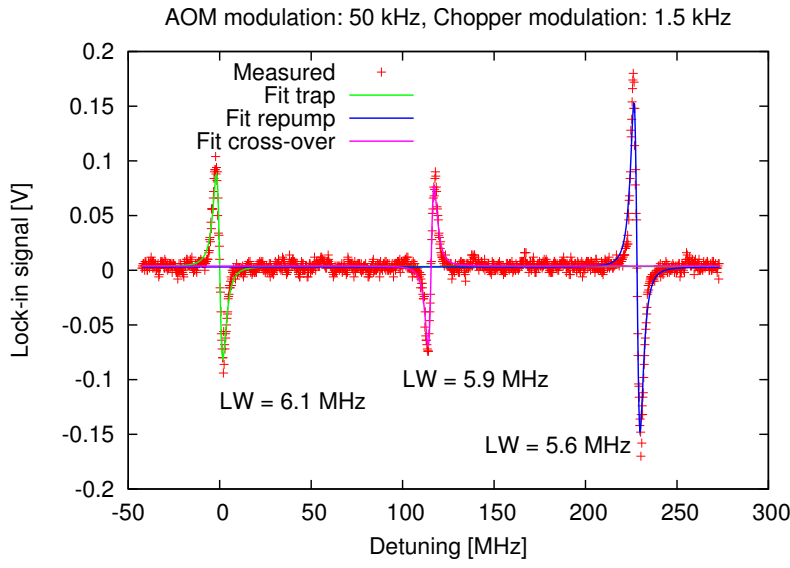


Figure 39: Doppler free spectrum without any DC offset. Another lock-in amplifier was added to the feedback loop to remove the DC offset in the error signal.

The following procedure locks the laser to the $2s - 3p$ transition:

- 1 Sweep the laser to acquire the Doppler-free spectrum. Adjust the center frequency of the laser to the zero-crossing of the trap error signal. Because the laser drifts, the signal will fluctuate about the peaks of the error signal.
- 2 Adjust the amplitude and offset of the cavity driver so that the cavity sweeps about the resonance. A scope capture of the error signal from the cavity is in Figure (40).
- 3 Lock the laser to the error signal from the Fabry-Pérot cavity.
- 4 Adjust the DC offset on the cavity to be at the center frequency of the trap signal from the heatpipe.
- 5 Lock the laser to the error signal from the heatpipe.

The laser is locked when the central frequency oscillates about the zero-crossing of the error signal. When the central frequency reaches either tail end of the error signal, the laser might become unlock. However, the integral gain in the PID accounts for this change and keeps the laser locked.

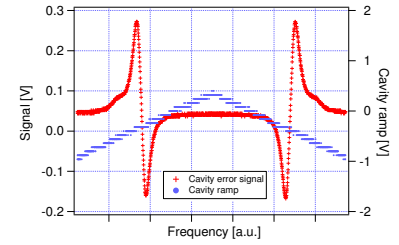


Figure 40: Error signal from Fabry-Pérot cavity. A triangle wave controlled the PZT which changed the length of the cavity. The laser was locked directly to the zero-crossing of the cavity error signal.

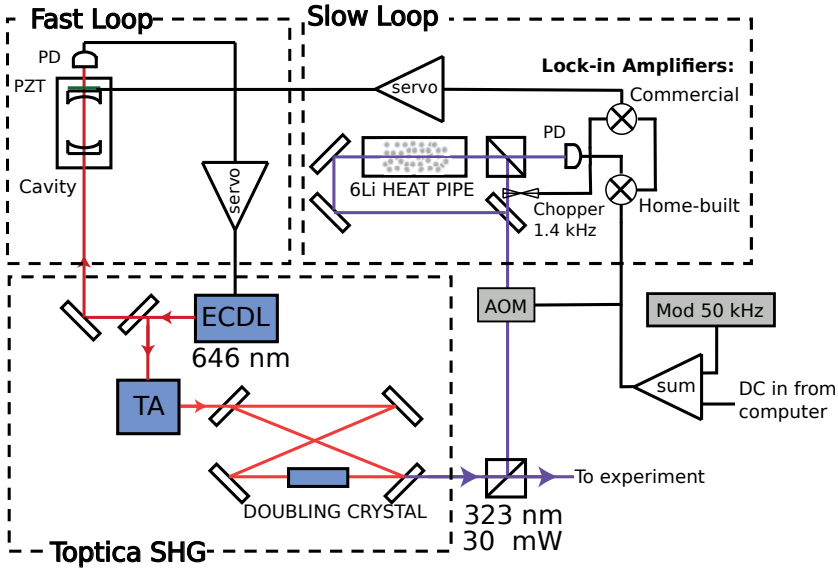


Figure 41: Schematic of the laser stabilization system. The Toptica ECDL provides 646 nm light that gets frequency doubled to 323 nm UV light. Part of the beam is sent to the experiment and the other part is sent to the laser lock system. The slow part of the lock consists of the two commercial lock-in amplifiers. The fast part consists of the Fabry-Pérot cavity. The compute provides a DC input which is added to the modulation signal.

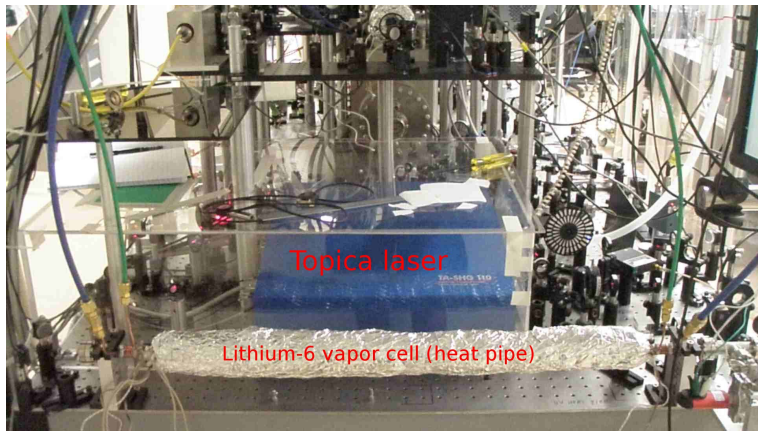


Figure 42: Picture of the lithium-6 vapor cell (heat pipe) with the Topica laser system in the background. The main part of the optical setup is to the right. The heat pipe oven was made by Pedro Duarte and Kevin Jourde. A major concern was to avoid having the lithium-6 vapor coating the windows of the cell, thereby reducing the laser beam transmission in the experiment. The solution was to wrap heaters around the center of the pipe and then water cool the ends. This setup allows the lithium-6 to vaporize in the middle of the cell and condense near the windows. The resulting pressure gradient creates a homogeneous gas since the vapor is forced from the center of the pipe to the edges. The total length of the heat pipe is about one meter.

Results

Introduction

The signal from the laser lock is presented in Figure (43). After locking the laser to the cavity, the DC offset on the cavity driver was set so that the laser frequency was at the center of the error signal zero-crossing. The lock was then engaged by sending the error signal back into the laser. The parameters on the PID were adjusted so that the noise on the error signal was minimized.

The error signal, along with the lock signal was recorded, as shown in the Figure on the next page. To produce this plot, the trap and crossover were also recorded to serve as a reference for the horizontal scaling. Because the crossover is in the middle of the trap and repump, the spacing between the trap and crossover is 114.1 MHz. The horizontal data for the trap and crossover was rescaled and fit to the first derivative of a Lorentzian, giving us the linewidth.

Assuming that the linewidth does not change, the zoomed in data for just the trap was re-scaled given the fitted linewidth. For an interval about the zero-crossing, the error signal was fit to a line thereby giving the corresponding change in frequency for a given change in voltage. The slope was found to be 127.64 mV/MHz. The bottom right inset shows the locked error signal. The fluctuations about zero correspond to the laser frequency oscillating about the zero-crossing of the error signal. The RMS locked linewidth was found to be 210 kHz, which is less than the linewidth of the $2s - 3p$ transition (~ 780 kHz). This locked linewidth should be acceptable for the ${}^6\text{Li}$ atom cooling experiment.

The stability of the lock was also tested. Under normal operating conditions, the lock was engaged and lasted all day until it was shut off. The stabilization system was impervious to events such as people gently closing (i.e. slamming) the doors. The laser was also able to lock when the pressure of the heat pipe doubled, which causes the error signal to diminish.

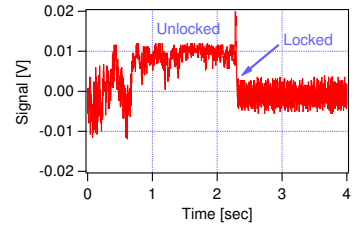


Figure 43: Scope capture of the laser stabilization with the home-built lock-in. Before the laser is locked, the signal drifts about the zero crossing of the error signal. Once the feedback to the laser is enabled, the laser locks to the zero crossing of the error signal. The noise is primarily due to the signal oscillating about the zero crossing of the error signal.

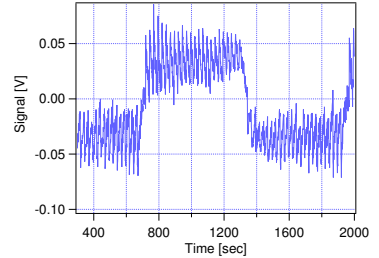


Figure 44: Lock signal with triangle signal. A triangle wave ($f = 0.2$ Hz, $V_{p-p} = 2$ V) with a DC offset of 5.0 V was fed into the DC input of the modulator circuit. The feedback system responded by continuously changing the laser frequency so that the laser stayed locked.

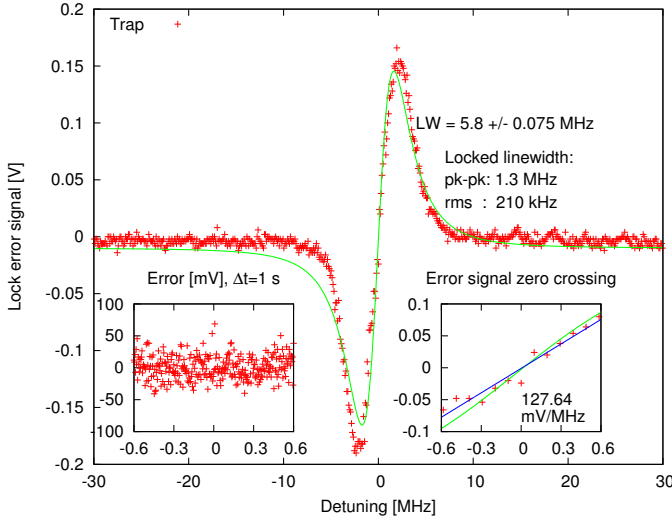


Figure 45: Data for the locked laser using the home-built lock-in and the commercial lock-in. The main figure shows the error signal fit to a Lorentzian. The bottom right inset shows a scope capture of the noise of the feedback signal sent into the laser. The bottom left inset shows the zero crossing of the error signal. A linear fit gives the slope used to convert the feedback signal (in mV) to frequency (in MHz).

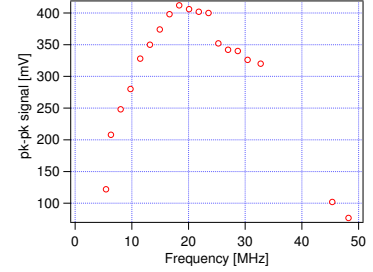


Figure 46: Tuning range of the lock. The AOM was aligned with the DC input of the modulation circuit set at 2.9 V. The DC offset was then changed from 1.1 V to 8.4 V and the pk-pk voltage was recorded for the trap signal. The lowest DC input voltage for the modulation circuit is about 2 V due to the circuit design. Also, the heatpipe had a relatively small temperature drift around $393 < T < 401$ (deg C) and the pressure was constant at about 4 mtorr.

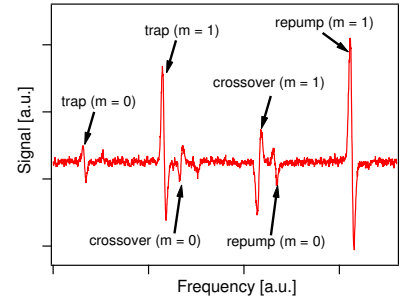


Figure 47: Error signals from the $m = 1$ and also the $m = 0$ order. The input DC signal was set to 8.4 volts. Since the AOM was aligned for the input DC signal of 2.9 V (arbitrary), the error signal from the zeroth-order is present, although much weaker than the first order.

³³ The units for electronic take this “strange” form because measurement instruments are normally calibrated in terms of a voltage or current. Since power \sim voltage², the noise level specified as an RMS voltage or current increases with the square root of the measurement bandwidth.

The rough tuning range of the lock was determined. As the DC input to the modulation circuit was varied, the amplitude of the error would also change, as shown in Figure (46). The DC input value was converted to frequency using the fit shown in Figure (31). The corresponding tuning range is 20 MHz. When the DC offset was increased to 8.4 V, the error signal from the $m = 0$ mode became observable as seen in Figure (47). To further test the lock stability, a triangle wave was added to the DC offset as shown in Figure (44). The lock started to become unstable when the pk-pk amplitude of the triangle wave was about 2 V. The laser also becomes unlocked when abruptly switching to the triangle wave from the constant DC offset.

To characterize the noise of the laser lock, a power spectrum was recorded as shown in Figure at the end of this section. The laser was stabilized to the $2s - 3p$ transition and then the lock error signal was sent into a spectrum analyzer (Standford Research Model SR780). The spectrum analyzer has a bandwidth of about 100 kHz. The horizontal axis was set to a log scale of the frequency. The vertical axis was set to RMS voltage per root Hertz ($V_{rms} / \sqrt{\text{Hz}}$)³³. As expected, the noise has a power spectral density function that follows as $S(f) \sim 1/f^a$ curve where f is the frequency in Hertz and a is about unity. There are peaks at ~ 1.5 kHz and ~ 50 kHz, which correspond to the chopper and AOM modulation, respectively. In addition, higher harmonics for the chopper signal are also present. No other major sources of noise were observed.

The laser lock can be improved in several ways:

1. **Locked linewidth reduction.** The locked linewidth is ultimately set by the fast and slow feedback in Toptica laser system itself. The fast feedback corresponds to direct current injection into the laser via a bias tee. The slow feedback consists of changing the laser current using FETs. For the setup used in this report, the slow part of the lock consists of the heatpipe error fed into a Fabry-Pérot cavity and then into the laser. The fast part consists of a doubling cavity error signal fed directly into the laser. To reduce the locked linewidth, the finesse of the Fabry-Pérot cavity needs to be increased. Cavities with a high finesse have sharp transmission so the laser will lock to a narrow error signal. Instead of using the error signal from the doubling cavity to feed into the fast part of the laser, use the error signal from the high finesse Fabry-Pérot cavity. This narrow signal fed into the fast feedback part of the laser leads to a narrower locked linewidth.
2. **Only modulate pump beam.** Without the chopper modulation of the pump beam, there is a temperature dependant DC offset in the ${}^6\text{Li}$ absorption spectrum. This DC offset comes from the residual amplitude modulation of the probe beam since the AOM modulates both the pump and probe beams. As the temperature of the heatpipe changes, the transmission of the probe beam changes as well. Because the DC offset in the absorption spectrum is proportional to the amplitude of the probe, there is a temperature dependant DC offset in the absorption spectrum. To remove this DC offset, we used a chopper to modulate the pump beam. Another possible solution would be to *only* modulate the pump beam with the AOM. Thus, the probe beam would not be modulated at all. The pump beam will then be at a different frequency than the probe, so the two beams will interact with different velocity group of atoms in the heatpipe. This requires that the AOM modulating the pump beam needs to be at a frequency such that both beams interact with the same velocity group. The beam for the atom cooling experiment interacts with atoms in the zero velocity group, so it would also need an AOM to change the beam frequency. However, for our setup, we would need an AOM at half the frequency of the AOM modulating the pump beam. Since we did not have such an AOM, we simply modulated both the pump and probe beams.
3. **Modulate atomic transitions.** Instead of modulating the pump and probe beams, we could modulate the atomic transition to generate an error signal. A homogeneous magnetic field around the heatpipe causes Zeeman splitting in the ${}^6\text{Li}$ energy levels. One could choose

a sub-level and then modulate the magnetic field. The magnitude of the magnetic field must be strong enough such that the splitting of the levels is greater than the linewidth of the transition. One would also have to consider the required frequency shift and how that corresponds to the change magnetic field. Experimental concerns would be how much current is necessary to generate the magnetic fields and the maximum modulation frequency of the magnetic field (limited by the induction in the coils).

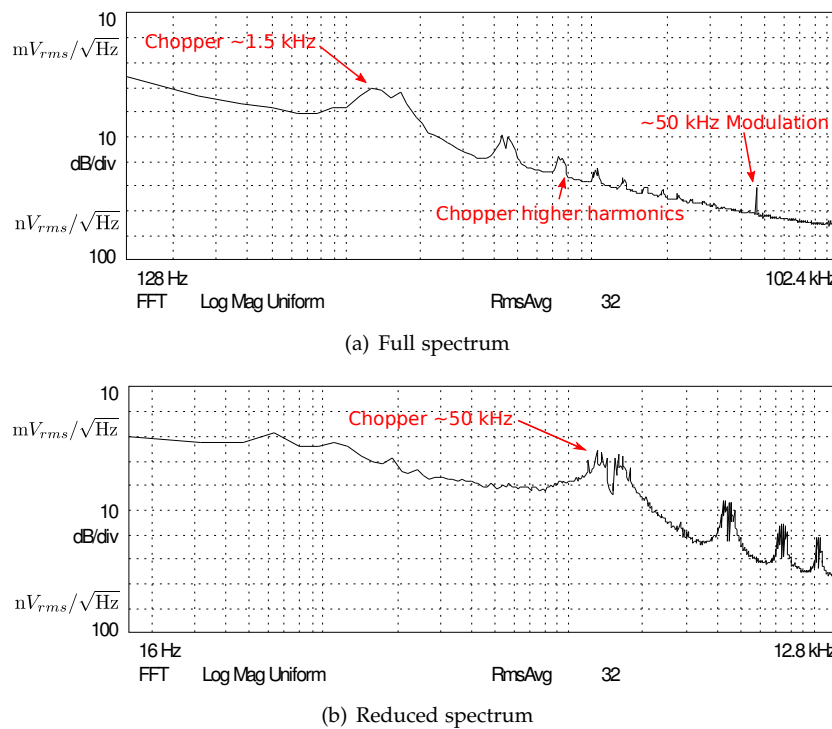


Figure 48: Power spectrum of the lock signal. The power spectral density is roughly inversely proportional to the frequency. (a) The signals from both the chopper and AOM modulation are present, along with some higher harmonics from the chopper signal. (b) Reduced span showing the chopper and higher harmonic signals.

Appendix

Parts and equipment list

List of parts	
Part	Description
Minicircuits SRA-6+	RF mixer for the lock-in
LF411	Garden variety op-amp
AD711	High-speed op-amp with $f_{GBW} = 4$ MHz
AD 797	Low noise preamp at audio bandwidths
AD 829	Low noise, highspeed op-amp for video applications
LM78Xx	Voltage regulators (National Semiconductor)
EXAR XR-2206	Monolithic function generator for the modulator
VCO	Linear tuning, 4.5 MHz/V (ZOS-100+)
Voltage Variable Attenuator	Bandwidth: 10-2500 MHz (ZX73-2500-S+) Max input power: 20 dBm
RF amp	

Equipment list	
Device	Description
Toptica laser	Second harmonic generation laser system (646/323 nm)
Cavity	Homemade Fabry-Pérot cavity
Wavelength Meter	Measures wavelength of laser (Bristol Instruments)
Spectrum Analyzer	For the wavemeter (Coherent Detector)
Vacuum pump	For the heat pipe (Varian Turbo-V 70)
Thorlabs DET25K	Photodiode for probe beam.
Lock-in Amp	Commercial lock-in amplifier (Signal Recovery Model 5105)
Spectrum Analyzer	Stanford Research Systems (SR780)
AOM	Bandwidth: 55-79 MHz centered at 67 MHz (IntraAction Corp. Model ASD-672B8)

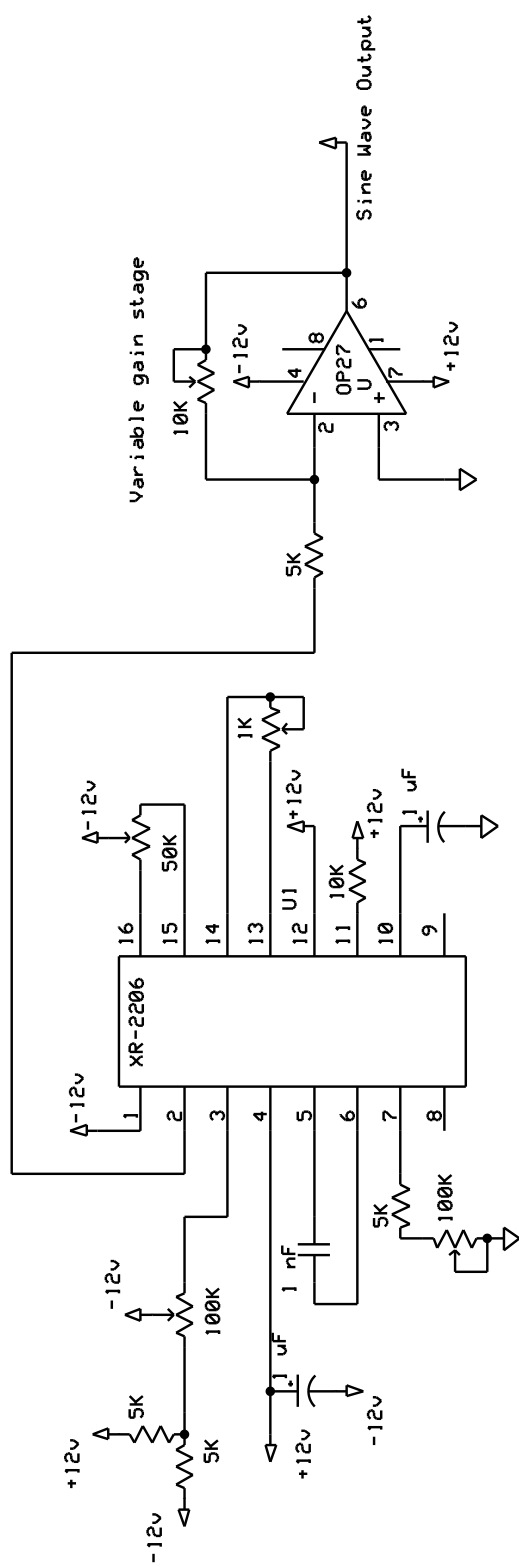


Figure 49: Modulation circuit. The XR-2206 is a monolithic function generator. The circuit is wired to produce a sinewave output. The capacitor across pins 5 and 6 along with the resistor at pin 7 determines the frequency of the signal.

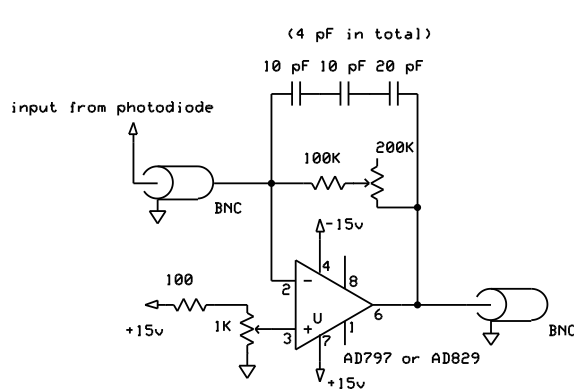
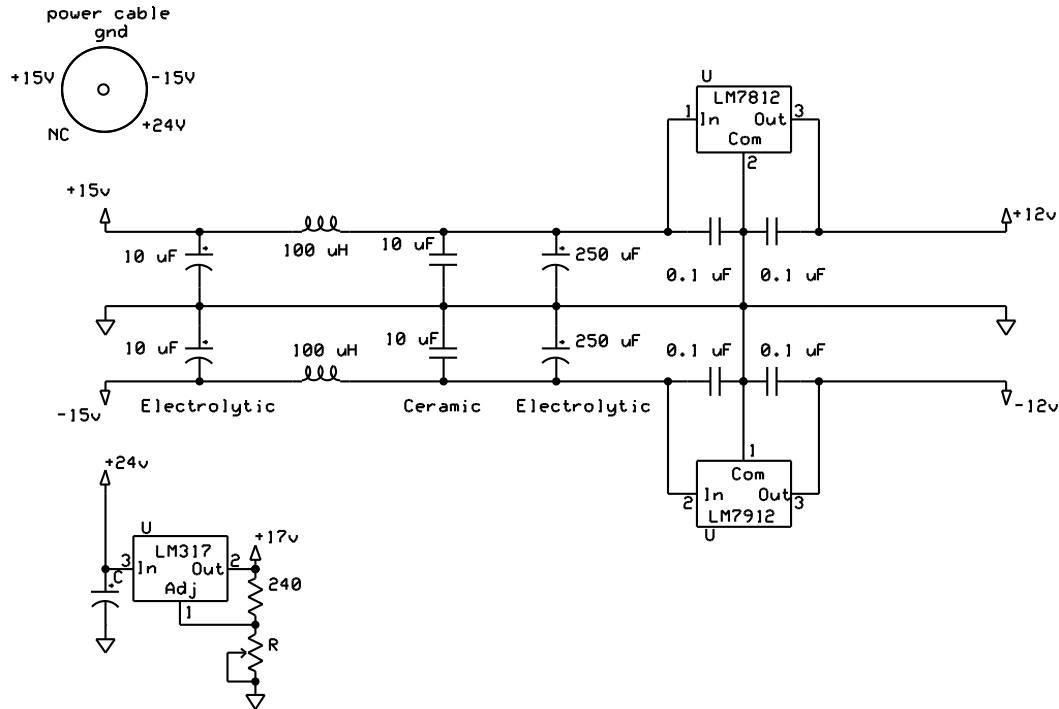


Figure 50: Power supply filter and voltage regulator for the modulation circuit. The input consists of +15V, ground, -15V, and +24V from a separate power supply. The capacitors serve to store energy during each voltage peak and release that energy when the supply voltage drops. The inductors, or *chokes*, resist instantaneous changes in current flow, thereby smoothing out ripples in the rectified waveform. Two voltage regulators take the filtered power and convert it to very stable output of +12, -12, and +17.5V.

Figure 51: Transimpedance amplifier used to amplify the signal from the photodetector. There is a pot for gain and also to adjust the offset.

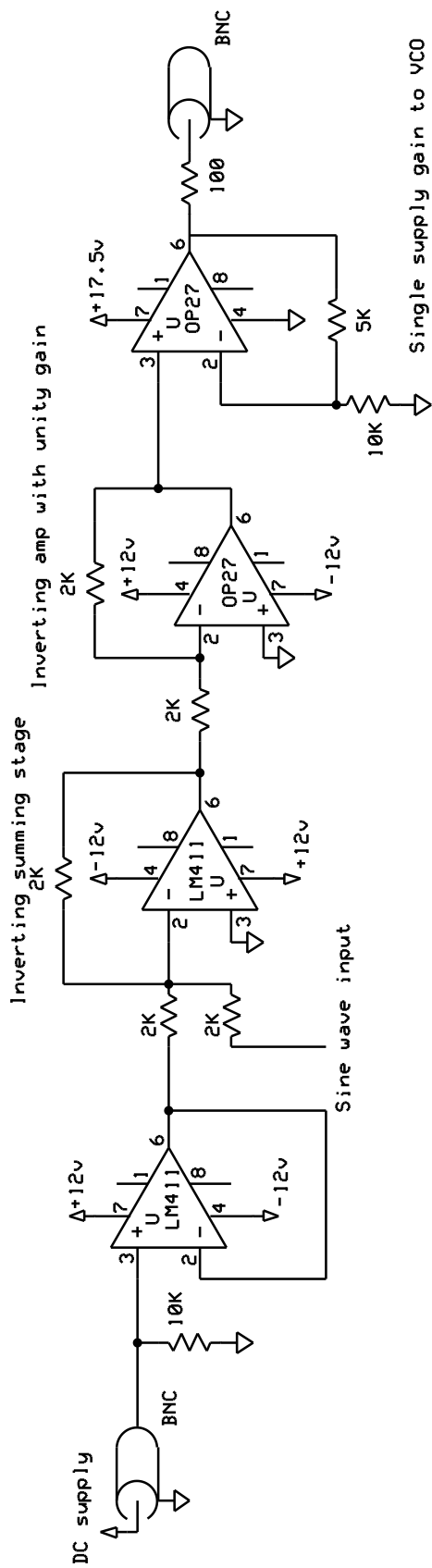


Figure 52: Summing circuit inside the modulator box. A DC signal from a computer is added to the modulation signal. There is an inverting amplifier of unitary gain because the summing stage is inverting. The output of the circuit goes to the VCO.

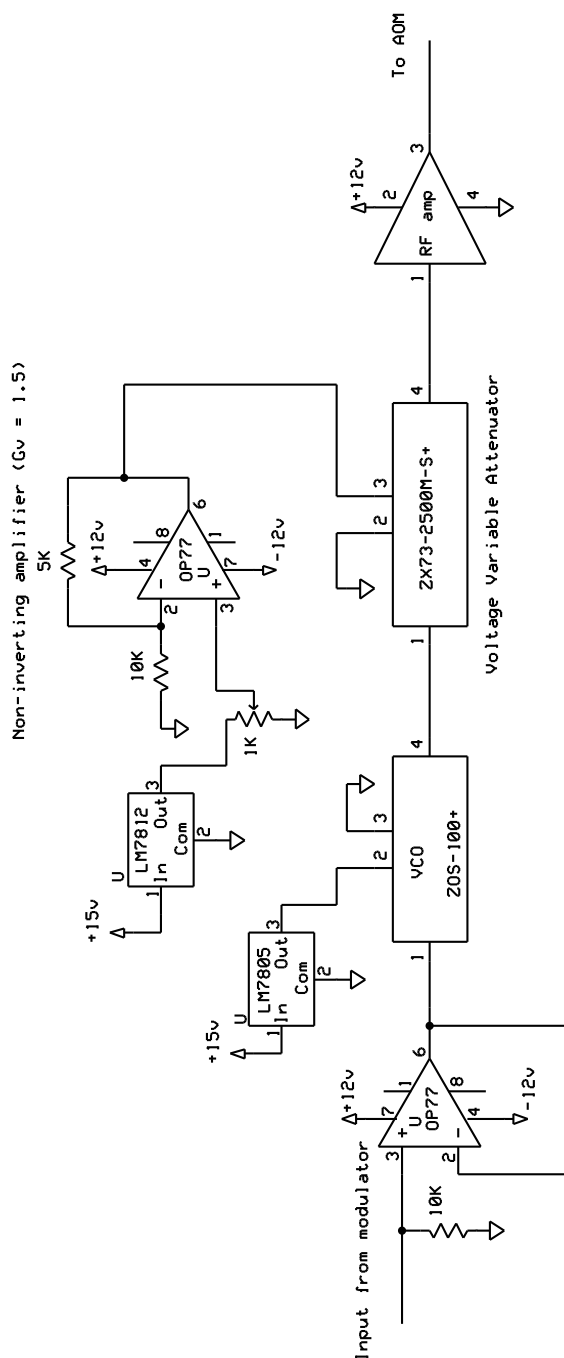
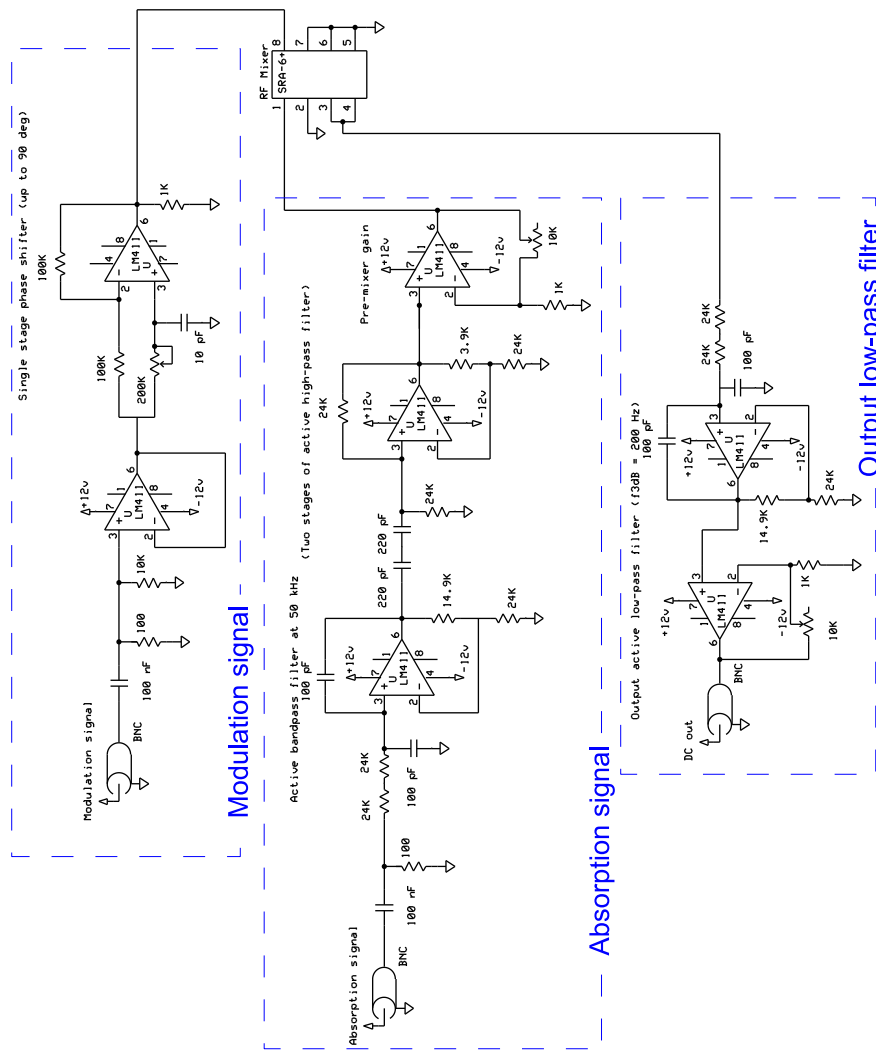


Figure 53: Voltage controlled oscillator and RF amplifier circuit for the AOM.

Figure 54: Demodulation circuit.



Bibliography

P. F. Bernath. *Spectra of Atoms and Molecules*. Oxford University Press, 2005.

Steven Chu. The manipulation of neutral particles, December 1997.

Claude N. Cohen-Tannoudji. Manipulating atoms with photons, December 1997.

J. Dalibard. *Journal of the Optical Society of America B*, page 2023, 1989.
DOI: [10.1029/2002JD002268](https://doi.org/10.1029/2002JD002268).

J. Dalibard. A home-built lock-in amplifier for laser frequency stabilization. *Can. J. Phys.*, 83:907–918, 2005.

John Emsley. *Nature's Building Blocks*. Oxford: Oxford University Press., 2001. ISBN 0198503415.

M. Greiner et al. *Nature*, 415:39–44, 2002.

Ralchenko et. al. Nist atomic spectra database. <http://physics.nist.gov/asd3>, 2010.

A. Filippov. *Z. Phys.*, 69:526, 1931.

C. J. Foot. *Atomic Physics*. Oxford University Press, 2005.

Harold Metcalf. *Laser Cooling and Trapping*. Springer, 1999.

Mini-Circuits. How to select a mixer, June 2008.

William D. Phillips. Laser cooling and trapping of neutral atoms, December 1997.

Adam Reed. Laser frequency stabilization for narrow linewidth cooling of ⁶Li atoms. American Physical Society Conference, Session W45, March 2011.

A. W. Weiss. *Astrophys. J.*, page 138, 1963.